Article

Cell Reports

The Chimpanzee SIV Envelope Trimer: Structure and Deployment as an HIV Vaccine Template

Graphical Abstract

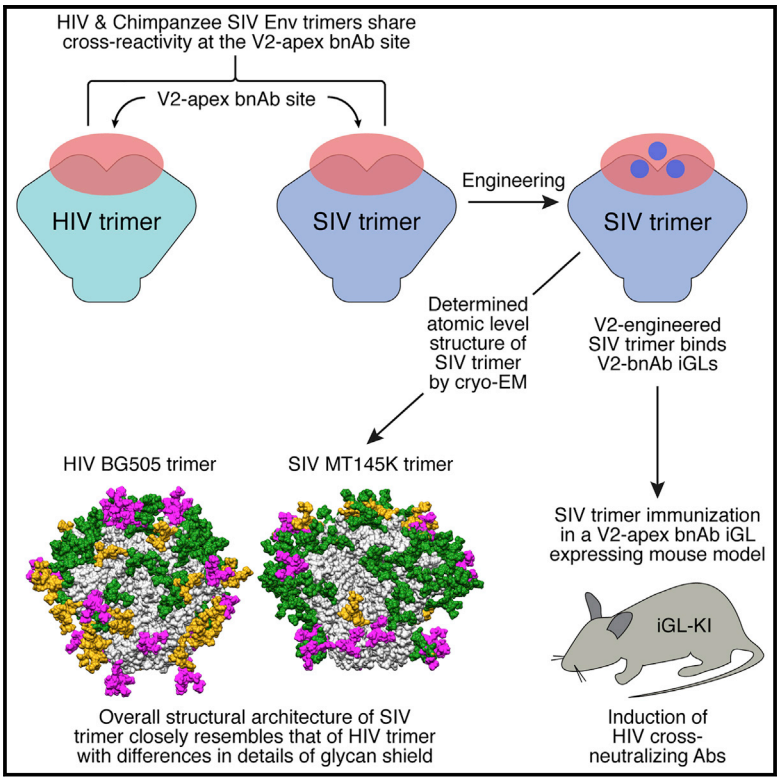

Highlights

- A designed chimpanzee SIV Env trimer binds HIV V2-apex bnAbs specifically
- The trimer (MT145K) is engineered to bind inferred unmutated versions of HIV V2-apex bnAbs
- The cryo-EM structure of the SIV MT145K trimer closely resembles that of HIV trimers
- The MT145K SIV trimer induces HIV-specific nAb responses in a favorable animal model

Authors

Raiees Andrabi, Jesper Pallesen, Joel D. Allen, ..., Laurent Verkoczy, Andrew B. Ward, Dennis R. Burton

Correspondence

andrew@scripps.edu (A.B.W.), burton@scripps.edu (D.R.B.)

In Brief

Design of immunogens and strategies that can induce protective broadly neutralizing antibodies (bnAbs) is a priority for HIV vaccine development. Andrabi et al. design a chimpanzee simian immunodeficiency virus (SIV) envelope trimer immunogen that binds specifically to HIV V2-apex bnAbs and their unmutated versions. The SIV trimer immunogen induces HIV-specific neutralizing antibodies (nAbs) in a favorable animal model.

Andrabi et al., 2019, Cell Reports *27*, 2426–2441
May 21, 2019
https://doi.org/10.1016/j.celrep.2019.04.082

CellPress

OPEN ACCESS
CellPress

Cell Reports
Article

The Chimpanzee SIV Envelope Trimer: Structure and Deployment as an HIV Vaccine Template

Raiees Andrabi,[1,2,3,13] Jesper Pallesen,[2,3,4,13] Joel D. Allen,[2,3,5] Ge Song,[1,2,3] Jinsong Zhang,[6,7] Natalia de Val,[2,4] Gavin Gegg,[1,2,3] Katelyn Porter,[1,2,3] Ching-Yao Su,[1,2,3] Matthias Pauthner,[1,2,3] Amanda Newman,[6,7] Hilary Bouton-Verville,[6,7] Fernando Garces,[2,4] Ian A. Wilson,[2,3,4,8] Max Crispin,[2,3,5] Beatrice H. Hahn,[9] Barton F. Haynes,[6,10] Laurent Verkoczy,[6,7,11] Andrew B. Ward,[2,3,4,14,*] and Dennis R. Burton[1,2,3,12,14,15,*]

[1]Department of Immunology and Microbiology, The Scripps Research Institute, La Jolla, CA 92037, USA
[2]International AIDS Vaccine Initiative, Neutralizing Antibody Center, The Scripps Research Institute, La Jolla, CA 92037, USA
[3]Center for HIV/AIDS Vaccine Immunology and Immunogen Discovery, The Scripps Research Institute, La Jolla, CA 92037, USA
[4]Department of Integrative Structural and Computational Biology, The Scripps Research Institute, La Jolla, CA 92037, USA
[5]School of Biological Sciences, University of Southampton, Southampton, UK
[6]Duke Human Vaccine Institute and Departments of Medicine and Immunology, Duke University School of Medicine, Durham, NC 27710, USA
[7]Department of Pathology, Duke University School of Medicine, Durham, NC 27710, USA
[8]Skaggs Institute for Chemical Biology, The Scripps Research Institute, La Jolla, CA 92037, USA
[9]Departments of Medicine and Microbiology, University of Pennsylvania, Philadelphia, PA 19104, USA
[10]Department of Immunology, Duke University School of Medicine, Durham, NC 27710, USA
[11]San Diego Biomedical Research Institute, San Diego, CA 92121, USA
[12]Ragon Institute of Massachusetts General Hospital, Massachusetts Institute of Technology, and Harvard University, Cambridge, MA 02114, USA
[13]These authors contributed equally
[14]Senior author
[15]Lead Contact
*Correspondence: andrew@scripps.edu (A.B.W.), burton@scripps.edu (D.R.B.)
https://doi.org/10.1016/j.celrep.2019.04.082

SUMMARY

Epitope-targeted HIV vaccine design seeks to focus antibody responses to broadly neutralizing antibody (bnAb) sites by sequential immunization. A chimpanzee simian immunodeficiency virus (SIV) envelope (Env) shares a single bnAb site, the variable loop 2 (V2)-apex, with HIV, suggesting its possible utility in an HIV immunization strategy. Here, we generate a chimpanzee SIV Env trimer, MT145K, which displays selective binding to HIV V2-apex bnAbs and precursor versions, but no binding to other HIV specificities. We determine the structure of the MT145K trimer by cryo-EM and show that its architecture is remarkably similar to HIV Env. Immunization of an HIV V2-apex bnAb precursor Ab-expressing knockin mouse with the chimpanzee MT145K trimer induces HIV V2-specific neutralizing responses. Subsequent boosting with an HIV trimer cocktail induces responses that exhibit some virus cross-neutralization. Overall, the chimpanzee MT145K trimer behaves as expected from design both *in vitro* and *in vivo* and is an attractive potential component of a sequential immunization regimen to induce V2-apex bnAbs.

INTRODUCTION

The ability to induce HIV envelope (Env) specific broadly neutralizing antibodies (bnAbs) will likely be a key feature of a prophylactic vaccine immunogen. Potent Env-specific bnAbs are produced in a small subset of HIV infected donors, yet attempts to elicit such responses through immunization have failed to date other than in certain animal models (Andrabi et al., 2018; Escolano et al., 2017; Escolano et al., 2016; Haynes and Mascola, 2017; McCoy et al., 2012; Sok et al., 2017; Xu et al., 2018). Previous studies have revealed that HIV bnAb germline-reverted precursors possess unique features that greatly reduce their overall frequencies in the human B cell immune repertoire and, hence, their ability to be targeted by vaccines (Briney et al., 2012; Haynes et al., 2012; Kepler et al., 2014; Klein et al., 2013; Verkoczy et al., 2010; Xiao et al., 2009). Therefore, recent immunogen design approaches that seek to induce bnAb responses by vaccination are taking these rare precursor features into consideration to efficiently activate bnAb precursors and shepherd them along favorable bnAb developmental pathways (Andrabi et al., 2015, 2018; Escolano et al., 2016; Gorman et al., 2016; Jardine et al., 2013; McGuire et al., 2013; Saunders et al., 2017; Steichen et al., 2016). These design approaches have shown promise for two of the HIV Env bnAb sites, namely the CD4 binding site (CD4bs) and the V3-N332 glycan site in animal models expressing the appropriate germline precursors (Andrabi et al., 2018; Briney et al., 2016; Dosenovic et al., 2015; Escolano et al., 2016; Jardine et al., 2015; McGuire et al., 2016; Sok et al., 2016a; Steichen et al., 2016; Tian et al., 2016; Williams et al., 2017). Thus, immunogen designs and strategies that can select rare bnAb precursors and reduce off-target B cell responses are valuable for nAb immunofocusing efforts.

One of the Env sites that has shown promise for vaccine targeting is the variable loop 2 (V2)-apex bnAb epitope (Andrabi et al., 2015; Gorman et al., 2016; Moore et al., 2017; Voss

et al., 2017). This bnAb epitope sits at the 3-fold axis of the trimer and is primarily formed by a patch rich in positively charged lysine residues and protected by two glycans at HXB2 HIV reference positions N160 and N156/N173 that are part of the Env glycan shield (Andrabi et al., 2017; Bhiman et al., 2015; Bonsignori et al., 2011; Doria-Rose et al., 2014; Gorman et al., 2016; Julien et al., 2013b; Lee et al., 2017; McLellan et al., 2011; Pancera et al., 2013; Walker et al., 2009, 2011). The bnAb precursors targeting this site possess a long anionic heavy-chain complementarity-determining region 3 (CDRH3) that penetrates the glycan shield to reach the protein epitope surface underneath (Bonsignori et al., 2011; Doria-Rose et al., 2014; Landais et al., 2017; Lee et al., 2017; McLellan et al., 2011; Walker et al., 2009, 2011). BnAb prototypes within this class interact with the V2-apex bnAb protein-glycan core epitope through common germline-encoded motifs and are, thus, targetable by a small set of trimers that interact with germline-reverted V2-apex bnAbs, as previously reported by us and others (Andrabi et al., 2015; Gorman et al., 2016). Hence, the germline-priming immunogens to this site could be based directly on native-like trimer configurations (Sanders et al., 2013, 2015). Other features that favor this site for vaccine targeting include the following: (1) V2-apex bnAbs are elicited frequently in humans that make bnAbs, (2) they emerge early in infection, and (3) they possess relatively low levels of somatic mutation compared to most other HIV Env bnAbs (Bonsignori et al., 2011; Doria-Rose et al., 2014; Georgiev et al., 2013; Kepler et al., 2014; Landais et al., 2016; Landais et al., 2017; Moore et al., 2011; Walker et al., 2009; Wibmer et al., 2013).

Of note, among the major HIV Env bnAb specificities, which include V2-apex, V3-N332, CD4bs, and the gp120-41 interface, the V2-apex is the only bnAb site that consistently exhibits cross-group neutralizing activity with virus Envs derived from HIV groups M, N, O, and P (Braibant et al., 2013; Morgand et al., 2016). Furthermore, V2-apex bnAbs display cross-neutralizing activity with the simian immunodeficiency virus (SIV) isolates that infect chimpanzees (SIVcpz*Ptt* [*Pan troglodytes troglodytes*], SIVcpz*Pts* [*Pan troglodytes schweinfurthii*]) and gorillas (SIVgor) (Barbian et al., 2015). The retention of the V2-apex bnAb epitope at the time of species crossover from chimpanzees to humans highlights the biological significance of this region and here we sought to design a trimer based on the SIVcpz*Ptt* Env sequence that could potentially help guide an immunofocused response to the HIV V2-apex bnAb site. We hypothesized that an SIVcpz*Ptt*-based trimer will not only assist in specifically enriching V2-apex-specific B cells but also, owing to V2-apex species cross-conservation, could assist in guiding a V2-focused nAb response when coupled with HIV trimers in a sequential prime-boost immunization strategy. In such an immunization scheme, the overall Env backbone sequence diversity in combination with conservation of the V2-apex bnAb epitope in sequentially administered immunogens is likely to reduce germinal center competition for V2-apex-specific B cells (Havenar-Daughton et al., 2017; Tas et al., 2016; Wang et al., 2015). Such a scheme could not only favor a B cell recall response to the V2-apex bnAb epitope but also reduce off-target Env-specific responses.

We designed an SIVcpz*Ptt*-based disulfide (SOS), I559P (IP) prefusion stabilized Env ectodomain truncated as residue 664 (SOSIP.664) trimer, MT145K, that displays native trimer-like properties, and selectively binds V2-apex bnAbs as well as their germline reverted precursor versions. We determined a structure of the MT145K trimer by cryo-EM at a global resolution of 4.1 Å and the overall architecture was remarkably similar to HIV Env trimers (Julien et al., 2013a; Lyumkis et al., 2013; Ozorowski et al., 2017; Pancera et al., 2014). In addition, the glycan shield composition of MT145K closely resembled that of HIV Env glycans but was sufficiently different in positioning of the glycans to exclude binding of all HIV bnAbs except for those directed to the V2-apex. MT145K trimer immunization in a V2-apex unmutated common ancestor (UCA)-expressing knockin mouse model revealed induction of a predominantly V2-apex neutralizing Ab response that was reproducible and cross-neutralized a related set of HIV isolates. Overall, the chimpanzee MT145K immunogen shows potential as an immunogen in HIV vaccination strategies.

RESULTS

Selection and Design of a Chimpanzee Env-Derived Trimer

Immunogen templates based on native-like Env trimers offer potential for HIV vaccine development, as they display bnAb epitopes and largely occlude non-native epitopes. However, it remains challenging to induce an epitope-focused bnAb response with Env trimer immunogens, as the bnAb epitopes are relatively immunoquiescent and even very limited exposure of non-desirable epitopes can negatively impact responses to bnAb epitopes (Havenar-Daughton et al., 2017; Wang et al., 2015). Therefore, trimer designs and/or strategies that can mask non-relevant immunodominant epitopes or reduce induction of off-target Ab responses could help guide immunofocused neutralizing responses. In addition, the typical lack of interaction of Env forms with germline-reverted bnAb precursors means difficulties in activating the appropriate B cell lineages. Accordingly, we undertook design of a trimer immunogen that could help guide an epitope-focused Ab response to the V2-apex site of HIV Env. Based on previous studies, we hypothesized that a chimpanzee SIVcpz*Ptt*/*Pts* or gorilla SIVgor Env sequence-based trimer that shares the V2-apex bnAb epitope with HIV could enrich B cell precursors and boost responses specific to this site (Barbian et al., 2015). Since SIVcpz*Ptt*, among various SIV-species Env sequences, are phylogenetically closest to the HIV Env, we surmised that the SOSIP.664 trimer-stabilizing modifications, which have been used on several HIV Env backgrounds, may function in the stabilization of soluble SIV Env (Gao et al., 1999; Sanders et al., 2013; Sharp and Hahn, 2011).

We incorporated the SOSIP.664 trimer design modifications into four SIVcpz*Ptt* Env sequences: GAB1, MB897, EK505, and MT145 (Figure S1). These isolates have been previously shown to be sensitive to the V2-apex bnAbs, PG9, PG16, and PGT145 (Barbian et al., 2015). Further characterization showed that one of these SIVcpz*Ptt* Env sequences, MT145 SOSIP.664, could be expressed as a soluble Env trimer protein (Figure S1). A PGT145 Ab affinity-purified MT145 trimer was efficiently cleaved into gp120 and gp41 subunits, and revealed well-ordered native-like

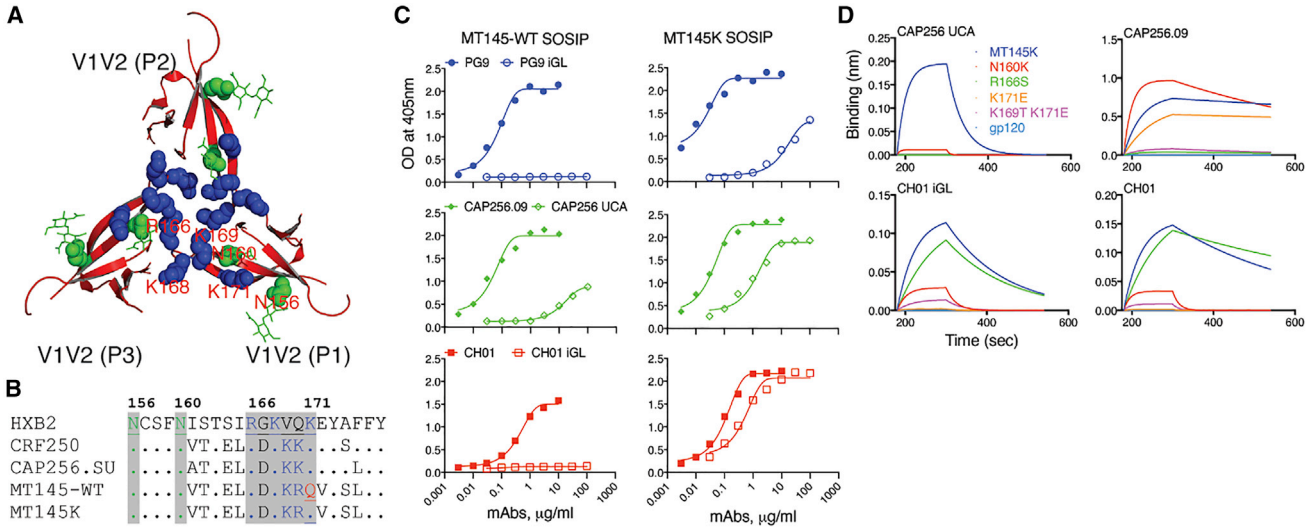

Figure 1. Design of a Chimpanzee Env-Stabilized Trimer and Binding to V2-Apex bnAb iGL Abs

(A) Structural arrangement of the V2-apex bnAb core epitope region on the BG505.664 soluble Env trimer (modified from Garces et al., 2015; PDB: 5CEZ). The ribbon representation of V1V2 loop strands that form the trimer apex show a cluster of positively charged lysine-rich peptide regions (HXB2-R166-K171: R or K residues shown as blue spheres) and the two glycans N156 and N160 (depicted in green spheres with lines). The side chains of the positively charged residues intersperse with the side chains of residues from adjacent protomers to form a continuous positively charged surface at the tip of the trimer to provide a minimal V2-apex bnAb epitope.

(B) Amino-acid sequence alignment of strand B and C V2 of HIV CRF250, CAP256.SU, chimpanzee SIV MT145 WT, and its V2-modified variant (Q171K), MT145K. Glutamine (Q) at position 171 (shown in red) was substituted with lysine (K) in MT145 Env to gain binding to V2-apex bnAb inferred germline (iGL) Abs.

(C) ELISA binding of mature V2-apex bnAbs, PG9, CAP256.09, and CH01 and their iGL versions to WT MT145 (red) and MT145K SOSIP trimers.

(D) Octet binding curves (association, 120 s [180–300]; dissociation, 240 s [300–540]) of CAP256 UCA and CH01 iGL Abs and their respective mature Ab versions (CAP256.09 and CH01) to MT145K trimer, its glycan knockout (N160K) variant, K-rich core epitope substituted variants, and the corresponding monomeric gp120. The Abs were immobilized on human IgG Fc capture biosensors and 1uM trimer or gp120 proteins used as analytes. The binding response is shown in nanometers (nm).

trimer configurations that were highly thermostable, which are all properties displayed by natively folded HIV soluble trimers (Figure S1) (Pugach et al., 2015; Sanders et al., 2013; Sharma et al., 2015).

Minimally Engineered MT145 (MT145K) Trimer Binds Prototype V2-Apex bnAb Precursors

One property thought to be critical for vaccine immunogens to select rare bnAb precursors is the ability to effectively bind to UCA B cell receptors (Dosenovic et al., 2015; Escolano et al., 2016; Jardine et al., 2015; McGuire et al., 2016; Steichen et al., 2016). Therefore, to gain or improve binding of the V2-apex bnAb inferred precursor Abs to the MT145 Env trimer, we substituted a glutamine (Q) with a lysine (K) residue (HXB2 position 171) in strand C of the V2-apex bnAb core epitope (Figures 1A and 1B). We based this substitution on the presence of a positively charged motif (KKKK) in CRF250 and CP256.SU strand C V2 Env sequences, both of which bind V2-apex bnAb prototype precursors (Andrabi et al., 2015; Bhiman et al., 2015; Doria-Rose et al., 2014; Gorman et al., 2016). ELISA binding revealed strong binding of the mature V2-apex bnAb prototypes with the MT145-WT trimer and weak but detectable binding with one of the UCA Abs, CAP256 UCA (Figure 1C). Strikingly, binding with our V2-engineered MT145 trimer (henceforth referred to as MT145K) not only improved binding to CAP256 UCA Ab but also conferred binding on both PG9 and CH01 inferred germline-reverted (iGL) Abs (Figure 1C). The PG9 and CH01 iGL Abs used here had diversity (D; heavy chain) and joining (J; both heavy and light chains) genes reverted to their corresponding germline gene families in the CDRH3s, in addition to the VH and VL regions reported previously (Andrabi et al., 2015; Gorman et al., 2016).

Previous mapping studies have defined the HIV core epitope recognized by mature V2-apex bnAbs (Andrabi et al., 2015; Gorman et al., 2016; Landais et al., 2017; Lee et al., 2017; McLellan et al., 2011; Pancera et al., 2013; Walker et al., 2009). To examine the contributions of V2-apex core epitope glycan and protein residues to binding by V2-apex bnAb iGL Ab versions, we generated MT145K strand C peptide and glycan trimer variants that are known to eliminate interactions of V2-apex bnAbs with the Env trimer (Andrabi et al., 2015; McLellan et al., 2011; Pancera et al., 2013). Bio-layer interferometry (BLI or octet) binding analyses of the iGL Abs with these trimer variants showed that glycan and/or peptide epitope requirements of precursor Abs were largely similar to the requirements of corresponding mature Abs (Figure 1D), suggesting that most contacts with the MT145K V2-apex core epitope are already encoded in the germline configuration for this class of bnAbs. Notably, the mature Abs showed slightly more tolerance to changes within the core protein epitope, particularly for the CAP256.09 bnAb, suggesting that part of the affinity maturation in this class of Abs may be to accommodate variation within the bnAb V2-apex core epitope.

Overall, the strand C V2-modification in the MT145 SOSIP.664 trimer conferred binding to multiple V2-apex bnAb germline prototypes.

Architecture of the MT145K Trimer

We solved the structure of the MT145K trimer by cryo-EM to a global resolution of ~4.1 Å (Figure S2; Table S1). To date, our structure represents the only atomic-level structure of an SIV Env trimer. Like other class I fusion proteins, protomers (gp120 and gp41) of MT145K trimerize to form a metastable pre-fusion Env trimer (Figures 2A, 2B, and S3) (Kwon et al., 2015; McLellan et al., 2013; Pallesen et al., 2016, 2017; Stevens et al., 2004). The trimer architecture exhibits a mushroom-like shape with subunits gp120 and gp41 constituting the envelope-distal and proximal entities, respectively (Figure 2B). Overall, the MT145K trimer configuration closely resembles that of the trimeric HIV Env spike, with an overall Cα root-mean-square deviation (RMSD) of 1.9 Å (Kwon et al., 2015). The arrangement of the V loops in the MT145K Env trimer is reminiscent of the V-loop arrangement in the HIV Env trimer and is suggestive of a similar role in immune evasion by steric occlusion of underlying conserved epitopes (Julien et al., 2013a; Pancera et al., 2014). Notably, the V1 and V2 loops are largely solvent exposed and occlude access to the underlying V3 loop (Figure 2C). Inaccessibility of the V3 loop is mediated by intra-protomer interactions of V1V2 to V3 and by extensive inter-protomer V1V2 trimer interactions at the apex of the spike. The SIV MT145K Env trimer exhibited well-ordered V2-V5 loops, while V1 is somewhat disordered (Figure 2D).

Proximal to the viral membrane is the gp41 subunit that forms the base of the trimer spike and is arranged into heptad repeat-1 (HR1), HR2, and the fusion peptide (FP) (Figure 2B). Similar to the HIV Env trimer, the three C-terminal helices of HR1 are centrally positioned along the trimer axis perpendicular to the viral membrane (Julien et al., 2013a; Lyumkis et al., 2013; Pancera et al., 2014). Intriguingly, the FP region, which has been observed to be solvent exposed on the outside of the HIV Env, is positioned in a pocket inside the MT145K trimer and remains sequestered in all three protomers (Figure 2E).

Conservation of the Glycan Shield on HIV and Chimpanzee SIV Env Trimers

To compare the nature of the glycan shield on SIVcpz*Ptt* Env and HIV Env, we performed site-specific glycan analysis of the MT145K trimer. The overall oligomannose content of the MT145K trimer is similar to HIV Env (Figures 3A and 3B) (Panico et al., 2016; Pritchard et al., 2015). However, although the distributions differ from the HIV clade A strain BG505, which is dominated by $Man_9GlcNAc_2$ oligomannose-type glycans, MT145K is predominantly $Man_8GlcNAc_2$ (Behrens et al., 2016). In addition, further processing was evident in the MT145K trimer, which showed elevated $Man_{6\text{-}7}GlcNAc_2$ structures (Figure 3B). The outer domain of gp120 presents a high density of oligomannose glycans that form the intrinsic mannose patch (Bonomelli et al., 2011), which is a highly conserved feature across the two viral species. The apex of the MT145K trimer possesses oligomannose-type glycans at N160 that correspond to the trimer-associated mannose patch (TAMP) also observed on HIV Env (Behrens et al., 2017). As for HIV, glycans at the base of the trimer at N88 and on gp41 of the MT145K trimer are extensively processed (Figures 3A and 3C).

The remarkable conservation in the overall architecture of the chimpanzee SIV and HIV Env glycan shield, despite sharing only ~62% of the amino-acid sequence identity, suggests that the glycan shield has an indispensable role in immune evasion and potentially maintaining the functional integrity of the trimer spike. Indeed, the glycan shield is integral to all lentiviral envelopes and appears to have evolved somewhat specifically to mammalian hosts (Figure S4). Over the course of lentiviral evolution, the Env glycan density shows an overall gradual progression and likely peaked in retroviruses infecting non-human primates and plateaued in HIV Envs (Figure S4) (Zhang et al., 2004). Therefore, the high-density Env glycan shield on HIV must have been established well before chimpanzee SIV crossed into humans. Nevertheless, several glycan positions on HIV Env appear to have subtly shifted after the species crossover: presumably as a result of adaptation to the human immune system (Figure S5).

MT145K Binds V2-Apex bnAbs Almost Exclusively

To define the overall antigenicity of the MT145K trimer, we first assessed the neutralization sensitivity of the MT145K virus (MT145-Q171K) to a broad panel of HIV Env-specific neutralizing and non-neutralizing (nnAbs) mAbs and compared these profiles to those for the clade A BG505 HIV virus (Figures 4A and S6) (Sanders et al., 2013; Voss et al., 2017). Remarkably, the V2-apex bnAbs, but essentially no other bnAbs or nnAbs (except 35O22 gp120-41 interface mAb), exhibited potent neutralizing activities against the MT145K virus (Figures 4A and S6). As previously observed, the BG505 isolate was sensitive to neutralization by all of the bnAbs in the panel, but none of the nnAbs (Figures 4A and S6).

Next, we evaluated binding of the MT145K trimer and monomeric gp120 to a panel of mAbs by ELISA and BLI. Consistent with the neutralization results above, bnAbs to the V2-apex site showed robust binding to the MT145K trimer (Figures 4B, S6, and S7), but other bnAbs and nnAbs did not bind, except for a few mAbs that displayed very weak binding (Figures 4B, S6, and S7). PG9, 17b, and some of the linear V3-loop directed mAbs (2557, 3074, 3904, and 14e) (Figures 4B and S6) displayed binding to the MT145K gp120 monomer. The results suggest that the sequence-dependent epitopes for some of the non-neutralizing V3-loop mAbs are present on monomeric MT145K gp120, but are obscured on the MT145K trimer, as indicated by the MT145K structure. Virus neutralization and trimer binding by mAbs is strongly correlated ($p = 0.003$), consistent with the notion that the MT145K soluble trimer adopts a native-like trimeric Env configuration and displays antigenic properties suitable for a vaccine immunogen.

HIV bnAb Epitopes on Chimpanzee SIV Env

To gain insight into the differences in the HIV Env bnAb epitopes on MT145K SIV Env that may potentially explain the reactivity of V2-apex bnAbs and non-reactivity of HIV bnAbs targeting other Env epitopes, we took advantage of the previously determined structures of human HIV bnAbs in complex with various HIV Env forms and compared the corresponding epitope regions

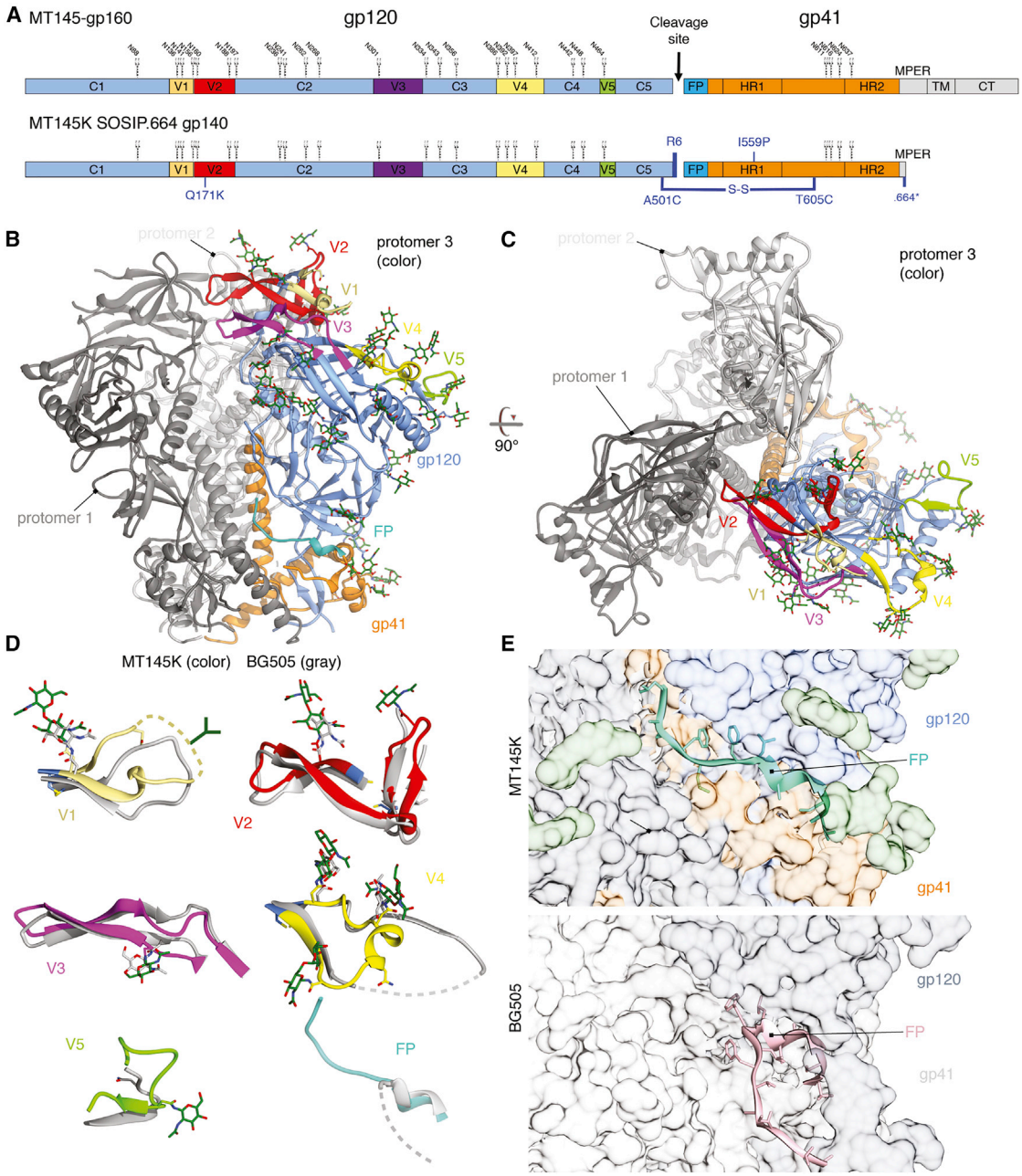

Figure 2. Cryo-EM Structure of the MT145K Trimer

(A) Schematic showing the MT145K SOSIP soluble trimer design from its full-length gp160 Env sequence. The gp120 constant (C1-C5) and variable (V1-V5) regions and the gp41 regions (fusion peptide, FP; heptad repeat, HR1 and HR2; membrane proximal external region, MPER; transmembrane, TM; and cytoplasmic tail, CT) are indicated. The N-linked glycan positions for each NXT or NXS residue are labeled according to the HIV HXB2 numbering scheme. The SOSIP trimer stabilizing modifications include (i) disulfide bond, A501C-T605C; (ii) R6 cleavage site; (iii) I559P; and (iv) 664-residue truncation in gp41 MPER. The substitution to incorporate a K residue at position 171 (Q171K) to gain binding for V2-apex iGL Abs is indicated in blue.

(B and C) Side (B) and top (C) views of the unliganded MT145K trimer model based on the cryo-EM density map at ~4.1-Å resolution. Ribbon representations of the MT145K trimer spike, in which the subunits gp120 (cornflower blue) and gp41 (orange) are depicted on one protomer. The gp120 variable loops (V1-V5) positioned to the trimer periphery are depicted in different colors (V1, khaki; V2, red; V3, magenta; V4, yellow; and V5, chartreuse). The fusion peptide region of gp41 is shown in cyan. Glycan sugar residues modeled based on density are represented in forest green stick form.

(D) Superimposition of variable loops (V1-V5) and fusion peptide region for MT145K and unliganded HIV clade A BG505 (PDB: 4ZMJ) SOSIP trimers. The dotted lines indicate regions in the V loops or FP for which the observed electron density was absent or unclear.

(E) Structural comparison of gp41 regions of the MT145K (orange) and BG505 (gray) trimers. The gp41 structural elements overall show a similar arrangement except for the fusion peptide region (colored cyan on MT145K and pink on BG505), which is exposed on the BG505 trimer but remains hidden in a pocket inside the MT145K trimer.

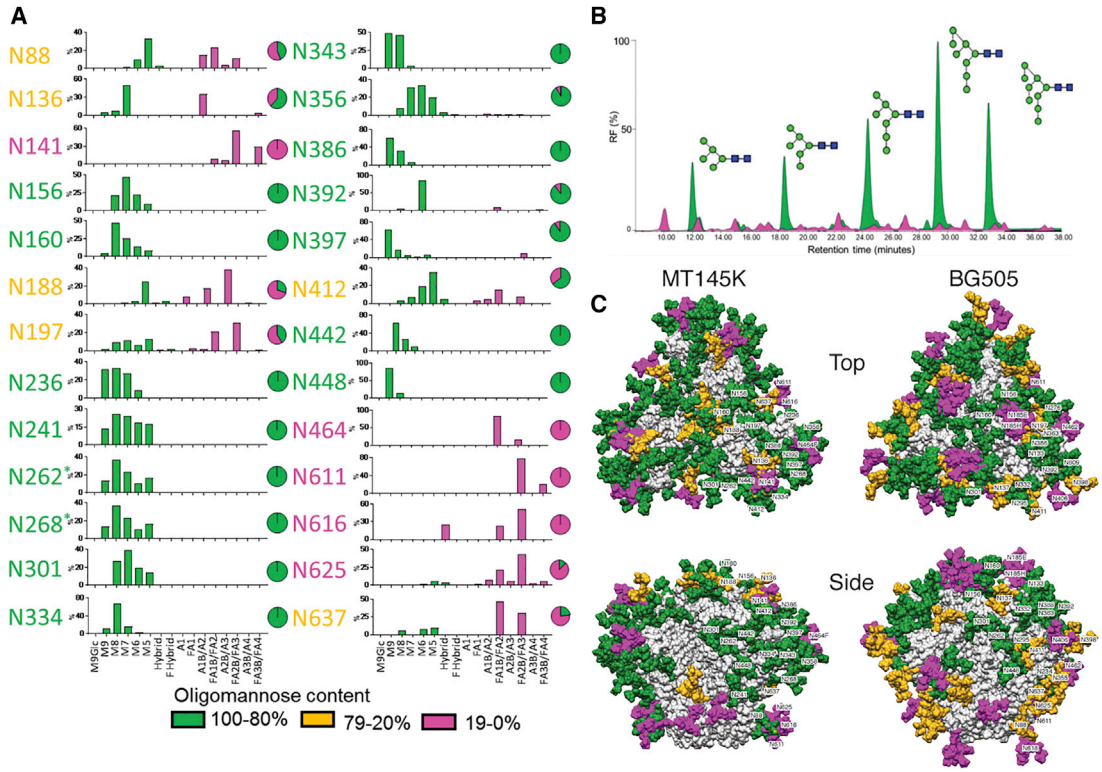

Figure 3. Site-Specific Glycoform Composition of MT145K Trimer

(A) Site-specific glycoform quantification of the MT145K SOSIP soluble trimer. MT145K trimers from transiently transfected HEK293F cell expressed supernatants were affinity purified by the quaternary trimer-specific antibody, PGT145. The purified MT145K trimers were treated separately with three proteases—trypsin, chymotrypsin, and elastase—and the digests were enriched for glycopeptides and analyzed by liquid chromatography-electrospray ionization mass spectrometry (LC-ESI MS). The individual glycan compositions of the N-linked glycan sites (n = 26) are represented by bar graphs that indicate the relative abundance of each glycoform species and are derived from the mean of two analytical replicates. The pie charts summarize the proportion of glycoforms for each site and this information is color coded: oligomannose type in green and complex and/or hybrid glycans in pink. The glycoforms at N262 and N268 positions (indicated by "*") could not be separately determined by enzymatic digestion and the bars represent the average glycan compositions across both sites.

(B) Hydrophilic interaction ultra-performance liquid chromatography (HILIC-UPLC) profiles of the total N-linked glycans released from the MT145K trimers. The proportions of oligomannose plus hybrid glycan contents and complex-type glycans are represented in green and pink colors, respectively.

(C) Modeled glycan shields for the MT145K and BG505 SOSIP trimers. Man9GlcNAc2 oligomannose-type glycans were docked and rigid-body fitted at each of the corresponding Env glycan positions using the MT145K structure (determined in this study [PDB: 6OHY]) and the unliganded BG505 SOSIP.664 trimer structure (Kwon et al., 2015; PDB: 4ZMJ). Top and side views of the trimers are shown and the individual glycan sites are labeled and color coded based on the content of oligomannose: green, 100%–80%; orange, 79%–20%; and pink, 19%–0%.

with those on the MT145K Env (Garces et al., 2014; Lee et al., 2016, 2017; Ozorowski et al., 2017; Pejchal et al., 2011; Wu et al., 2010). A lysine-rich patch in strand C of the V2 loop (^{166}RDKKQK^{171} on BG505 Env) and two nearby glycans N160 and N156 form the core epitope for V2-apex bnAbs on HIV Envs (Figures 5A and S8) (Gorman et al., 2016; Julien et al., 2013b; Lee et al., 2017; McLellan et al., 2011; Pancera et al., 2013). Both of these features are conserved on the MT145K trimer, thus enabling the human V2-apex bnAbs to be effective against the SIV Envs (Figures 5A, S5, and S8) (Barbian et al., 2015).

Binding of one of the V3-N332 epitope-specific bnAbs, PGT128, predominantly relies on the N332 glycan and a neighboring peptide motif ^{324}GDIR^{327} at the base of the V3 loop (Figures 5B and S8) (Garces et al., 2014; Gristick et al., 2016; Kong et al., 2013; Pejchal et al., 2011; Sok et al., 2016b). The lack of binding to the MT145K trimer by PGT128 and other bnAbs in this class can be explained by the absence of the N332 glycan on this Env. In contrast, three of the four core protein epitope residues ^{324}G-^{325}D-^{327}R are conserved on the MT145K trimer and, in fact, on other chimpanzee SIV Envs (Figures 5B, S5, and S8). For the PGT128 class bnAbs, the interaction with glycan N332 can be substituted by the N295 glycan observed in some HIV isolates, but not by glycan N334 that is present on the MT145K trimer (Sok et al., 2014a). In fact, the MT145K N334 glycan is positioned in a direction away from the V3-N332 epitope site, making it impossible to facilitate bnAb binding to this epitope. Strikingly, the majority of the known SIVcpz Env sequences possess an N334 glycan in place of the more common N332 glycan on the HIV Env, which appears to be a significant glycan shift upon species crossover as the virus established itself in humans (Figure S5). In addition, the glycans at N442 in the gp120-C4 region and N412 in the gp120-V4 region of MT145K Env may obstruct PGT128 binding. The glycan at N442, unique

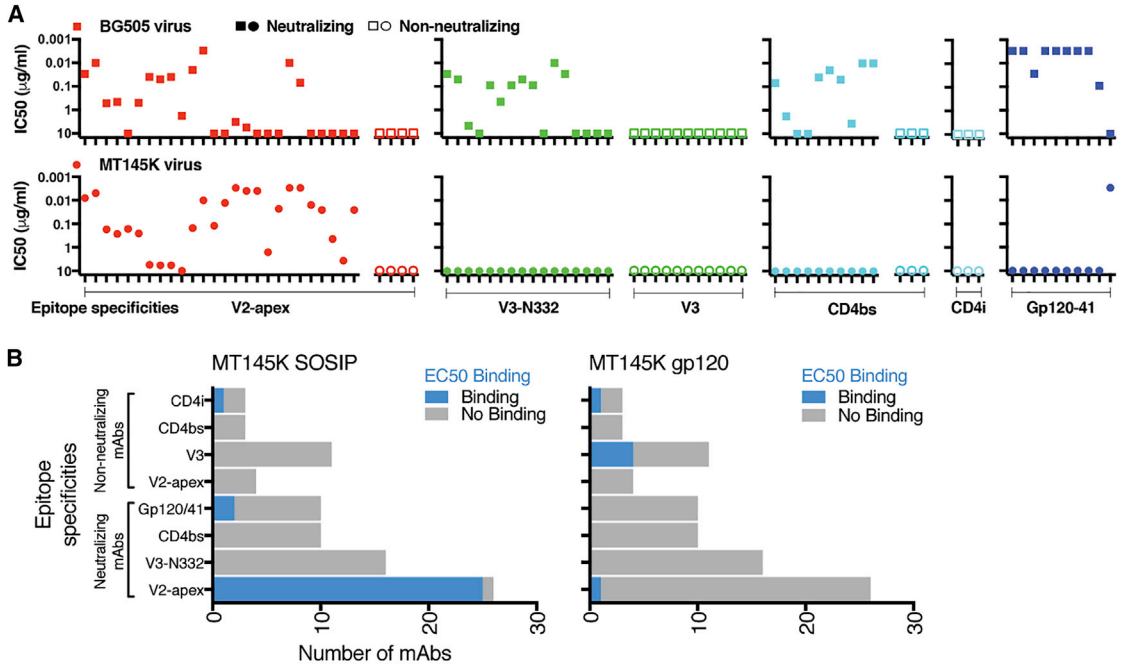

Figure 4. Antigenic Profile of the MT145K Trimer

(A) HIV Env-specific mAbs were used to characterize the antigenicity of the MT145K Env trimer. MAbs targeting neutralizing and non-neutralizing epitope specificities, including V2-apex, V3-N332, linear V3, CD4bs, CD4i, and the gp120-41 interface were tested with MT145K and BG505 Env-encoding pseudoviruses in a TZM-bl cell-based reporter assay. The reciprocal IC_{50} neutralization titers for each virus are indicated as dot plots; plots for individual epitope specificities are depicted separately. The neutralization sensitivity comparison of BG505 and MT145K viruses against the mAb panel shows a selectively potent neutralization of MT145K by V2-apex bnAbs but no other bnAbs, except a single gp120-gp41 interface bnAb, 35022. The BG505 virus was neutralized by bnAbs targeting diverse Env sites.

(B) The above mAb panel was further tested with PGT145 Ab-purified MT145K trimer and Galanthus nivalis lectin (GNL)-purified MT145K gp120 monomer by ELISA. The binding, represented as EC_{50} binding titers, shows selective binding of MT145K by V2-apex bnAbs. Two of the gp120-gp41 interface bnAbs and a CD4i mAb also showed significant binding to the MT145K trimer. Four of the non-neutralizing mAbs specific to a linear V3 epitope exhibited binding to MT145K gp120, but not to the trimer.

to the MT145K Env trimer and several other SIVcpz Envs, may clash with CDRH2 of PGT128 and perhaps other bnAbs in this class and may prevent them from accessing the epitope (Figures 5B and S5).

PGT151 represents another glycan-targeting bnAb class (Blattner et al., 2014; Falkowska et al., 2014; Lee et al., 2016) that recognizes several glycans on gp120 (N88 and N448) and gp41 (N611 and N637), as well as the fusion peptide. All glycans and fusion peptide residues that contribute to the PGT151 epitope are conserved between HIV and SIVcpz Envs (Figure S5). Therefore, the lack of PGT151 binding to MT145K is most likely attributable to inaccessibility of the FP on MT145K (Figure 5C).

The CD4bs is conserved between HIV and SIV to the extent that there is cross-species reactivity with sCD4. Human CD4-IgG2 immunoadhesin showed strong binding to the MT145K trimer, indicating a strong cross-species conservation of the Env CD4bs. Phe43 in domain-1 of human sCD4 would fit well inside the Trp427 Env cavity on the MT145K trimer, reminiscent of its interaction with the HIV Env BG505 trimer (Figure 5D) (Ozorowski et al., 2017). However, the MT145K trimer is non-reactive with CD4bs bnAbs. VRC01, one of the bnAbs in this class, binds to the HIV Env CD4bs bnAb epitope formed by discontinuous protein backbone elements including loop D of the gp120-C2 region and bordered by a glycan at N276 (Figures 5E, 5F, S5, and S8) (Wu et al., 2010). MT145K lacks the N276 glycan and the proximal N234 glycan, present in most HIV Envs, but instead has a glycan at position 236. Differences in the loop D sequence (Figure S5) and the glycan at N236, which may clash with VRC01 CDRL1 and CDRL3 loops (Figure 5F), on the MT145K trimer likely impose the biggest impediment to VRC01 binding. Further, the MT145K gp120-V5 loop has a six-amino-acid insertion at HXB2 position 456 compared to HIV Envs that may clash with the VRC01 LC (Figures 5F and S5).

Overall, the non-reactivity of HIV Env bnAbs with the MT145K trimer can be largely ascribed to subtle glycan shifts that have occurred in HIV from chimpanzee SIV Env as the virus established itself in humans.

The Engineered MT145K but Not the MT145-WT Trimer Activates V2-Apex UCA-Expressing B Cell Precursors *In Vivo*

To determine whether the engineered chimpanzee MT145K trimer could efficiently activate HIV V2-apex Ab germline-encoding precursor B cells *in vivo* and how it compares with the MT145-WT trimer, we conducted immunization experiments in the CH01 UCA "HC only" knockin (KI) mouse model. This

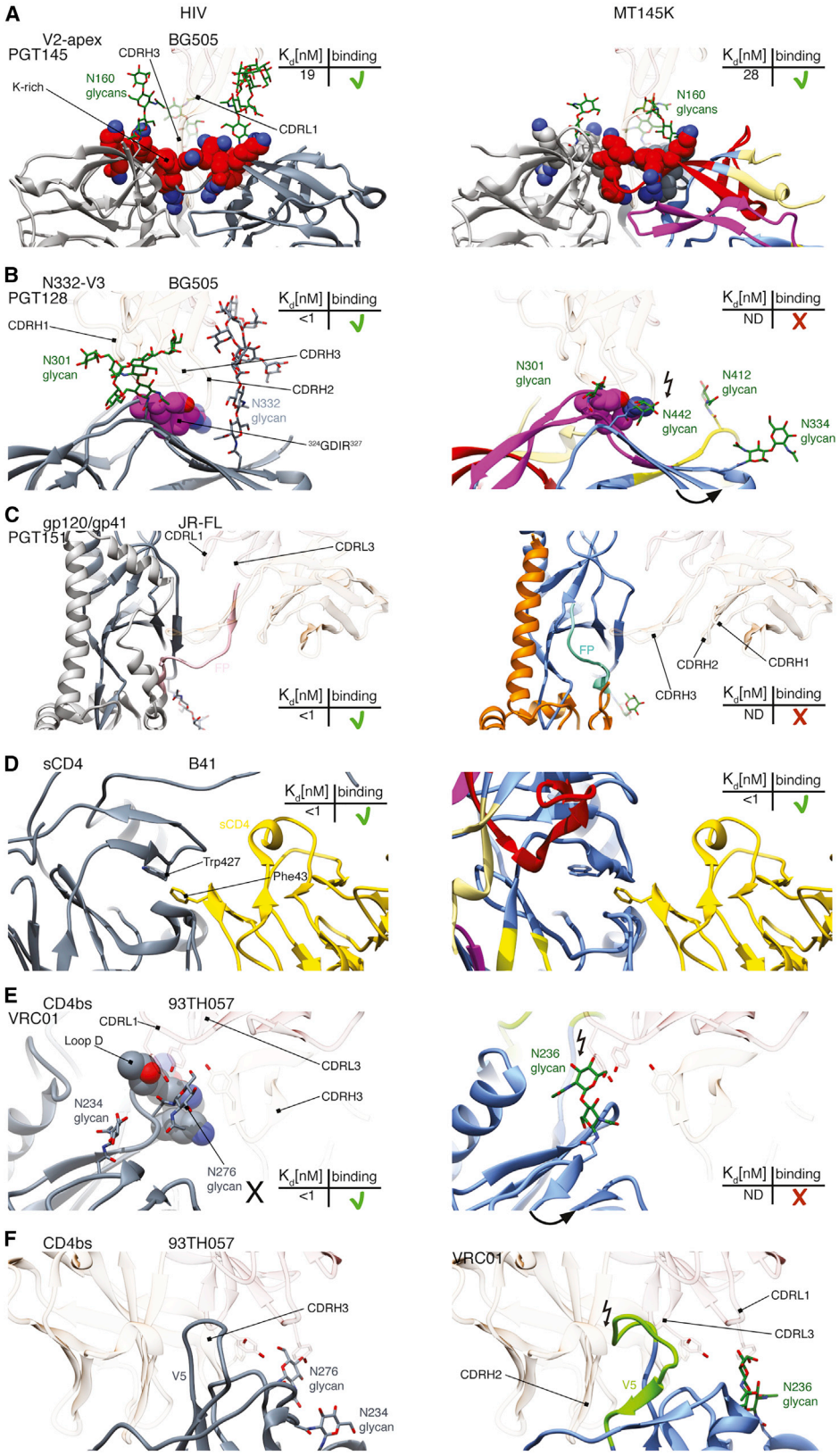

(legend on next page)

KI-mouse model expresses the pre-rearranged heavy chain (V_HDDJ_H) of the CH01 V2-apex bnAb UCA paired with wild-type (WT) mouse light chains. We immunized two groups of five CH01 UCA heavy chain (HC)-only KI mice, each with two repeated doses (at weeks 0 and 4) of the MT145-WT or MT145K trimer (Figure 6A). To track the development of Ab responses, we performed ELISA assays of the pre-bleed, 2-week (day 14) post-prime (Bleed #1) and 2-week post boost-1 (day 42) (Bleed #2) serum samples with MT145K SOSIP trimer protein and its N160-glycan-eliminated variant (MT145K N160K) (Figure 6B). The N160 glycan is a critical component of the V2-apex bnAb epitope (Lee et al., 2017; McLellan et al., 2011; Pancera et al., 2013; Walker et al., 2009). The pre-bleed serum samples in both immunization groups exhibited weak binding activity with the MT145K trimer that was dependent on the N160 glycan, consistent with the presence of CH01 UCA Abs that do show some binding to the MT145K trimer, as described above (Figure 6B).

The immunogen-specific titers of the serum Ab responses post-prime immunizations (Bleed #1 samples) marginally increased in the MT145K group but remained largely unchanged in the MT145-WT trimer immunized group. The serum Ab titers post-boost-1 immunization (Bleed #2) increased in both the groups and were orders of magnitude higher as compared to the pre-bleed or the post-prime Ab binding responses (Figure 6B). At this immunization step, the serum Ab responses in the MT145K trimer immunized group were solely dependent on the N160 glycan while those in the MT145-WT trimer immunization group were mostly independent of the N160 glycan (Figure 6B). Therefore, we conclude that the engineered MT145K trimer, but not the MT145-WT, efficiently triggers the epitope-specific V2-apex bnAb UCA encoding B cell precursors *in vivo*. Remarkably, immunizations with the Q171K-substituted engineered MT145K trimer also appeared to eliminate the non-V2-apex bnAb site Env-specific off-target B cell responses that were elicited in the MT145-WT trimer immunization group (Figure 6B). The results demonstrate that the activation of the HIV Env bnAb-encoding unmutated B cell precursor by immunogens that display binding to their UCA Ab versions is critical for eliciting epitope-specific Ab responses and the findings are consistent with studies that specifically use germline-targeting immunogen molecules to kick off the bnAb precursor encoding B cell responses *in vivo* (Dosenovic et al., 2015; Escolano et al., 2016; Jardine et al., 2015; McGuire et al., 2013; Sok et al., 2016a; Steichen et al., 2016; Tian et al., 2016).

Next, we evaluated immune sera for neutralization of autologous and heterologous viruses. Reproducible MT145K autologous virus-specific neutralizing Ab responses were induced in the MT145K immunization group but not in the MT145-WT immunization group (Figures 6C and 6D). As for the ELISA binding responses, the nAb titers in the MT145K trimer immunized group increased at 2 weeks post prime, as indicated by nAb titers against a highly CH01-sensitive HIV Env-encoding virus (Q23_17) and, further, markedly increased after the boost-1 immunization (Figure 6C). At this point, all animals in the MT145K group developed autologous virus-specific nAb responses (Figure 6C). The nAb responses in MT145K trimer-immunized animals mapped to the glycan N160 and strand C K171 residue, both of which form part of the core epitope for V2-apex bnAbs, suggesting that the MT145K trimer successfully primed V2-apex UCA B cells in an epitope-specific manner *in vivo*.

Overall, we conclude that the engineered chimpanzee MT145K but not the MT145-WT trimer activated the V2-apex-specific bnAb precursor B cells in a UCA-expressing mouse model.

HIV Trimer Cocktail Boosting Recalls Chimpanzee MT145K Trimer-Induced V2-Apex B Cell Responses in the CH01 UCA Model

Evaluation of the utility of the MT145K trimer in a sequential HIV immunization regime will be best carried out in humans. Nevertheless, we were interested to investigate if the chimpanzee SIV MT145K trimer-induced B cell responses could be boosted by HIV trimers that share conservation at the V2-apex bnAb site

Figure 5. A Close-Up View of Regions on the MT145K Trimer That Correspond to Those Recognized by HIV bnAbs on HIV Trimers

(A) V2-apex bnAb binding region: cryo-EM model of PGT145 bnAb (HC, transparent sandy brown; LC, transparent orchid) in complex with the BG505 SOSIP trimer depicting V1V2 loops in ribbon representation (Lee et al., 2017; PDB: 5V8L). The strand C K-rich region (^{166}RDKKQK^{171}; red spheres) and the glycan N160 (forest green sticks) that form the epitope for PGT145 bnAb are indicated. The elements in the core epitope interact with the CDRL1 loop and the long CDRH3 loop that penetrates through glycans to reach the positively charged surface underneath. Both glycan N160 and the positively charged protein residues are conserved between BG505 HIV and MT145K SIV Env trimers.

(B) V3-glycan bnAb binding region: cryo-EM model of PGT128 bnAb (HC, transparent sandy brown; LC, transparent orchid) in complex with the BG505 SOSIP trimer (Lee et al., 2015; PDB: 5ACO). The V3 loop protein backbone residues (^{324}GDIR^{327}; depicted in purple spheres) and the glycans N301 and N332 form the bnAb epitope and are shown to interact with the antibody CDR loops. The MT145K trimer has a glycan at N334 rather than N332 and the glycan points away from the expected location of the PGT128 Ab paratope. In addition, MT145K Env has glycans at two positions, N412 (positioned differently on HIV Env) and N442 (absent on HIV Envs), and particularly the latter will clash with PGT128 CDRH2 and prevent it from interacting with the protein part of the epitope.

(C) The gp120-gp41 interface bnAb binding region: cryo-EM model of PGT151 bnAb bound to a membrane-extracted clade B JRFL Env trimer. The structure depicts PGT151 bnAb CDRs interacting with gp120 and the gp41 interface regions (Lee et al., 2016; PDB: 5FUU). PGT151 CDRH3 interacts with the epitope formed by the protein backbone (in both gp120 and gp41), including the fusion peptide (depicted in pink) and the gp120 (N88, N448) and gp41 (N611 and N637) glycans (not shown). PGT151 Ab CDR loops interact with the FP region on the BG505 trimer. The MT145K trimer FP region (cyan) remains hidden inside the trimer.

(D) Cryo-EM model of two-domain human sCD4 with the B41 SOSIP trimer (Ozorowski et al., 2017; PDB: 5VN3). The structure shows how the Phe43 residue on sCD4 stacks into the Env cavity lining Trp427. This Trp427 cavity is conserved between HIV and MT145K Envs to accommodate CD4 binding.

(E and F) The CD4bs bnAb binding region: crystal structure of VRC01 bnAb in complex with 93TH057 gp120 (Zhou et al., 2010; PDB: 3NGB). The structure depicts VRC01 CDRH3, CDRL3, and CDRL1 loops interacting with the protein residues in loop D (HXB2: 278-282) and the glycan at N276 (E and F, left panels). The MT145K trimer lacks the N276 glycan and bears glycan N236 (unique to SIV Env) in place of N234 that would clash with the VRC01 CDRL1 loop (E and F, right panels). Additionally, the MT145K Env trimer has a longer gp120-V5 loop due to a six-amino-acid insertion at HIV HXB2-456 residue that would shift the loop such that it clashes with the CDRH2 the VRC01 Ab.

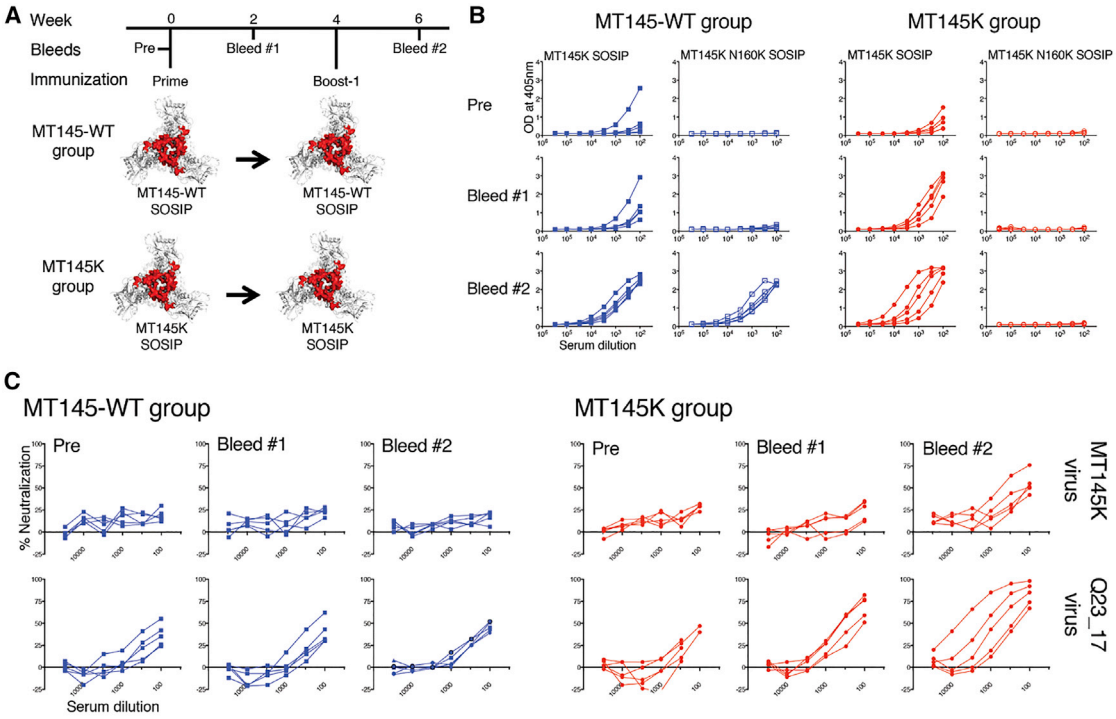

D

	MT145-WT group														
	Pre-bleed					Bleed #1					Bleed #2				
Virus/mutant	13315	13316	13317	13318	13319	13315	13316	13317	13318	13319	13315	13316	13317	13318	13319
MT145K	<100	<100	<100	<100	<100	<100	<100	<100	<100	<100	<100	<100	<100	<100	<100
MT145K N160A	<100	<100	<100	<100	<100	<100	<100	<100	<100	<100	<100	<100	<100	<100	<100
MT145-WT	<100	<100	<100	<100	<100	<100	<100	<100	<100	<100	<100	<100	<100	<100	<100
Q23_17	<100	150	<100	<100	<100	<100	<100	<100	<100	160	<100	<100	<100	<100	<100

	MT145K group														
	Pre-bleed					Bleed #1					Bleed #2				
Virus/mutant	13200	13201	13202	13300	13301	13200	13201	13202	13300	13301	13200	13201	13202	13300	13301
MT145K	<100	<100	<100	<100	<100	<100	<100	<100	<100	<100	109	121	<100	135	576
MT145K N160A	<100	<100	<100	<100	<100	<100	<100	<100	<100	<100	<100	<100	<100	<100	<100
MT145-WT	<100	<100	<100	<100	<100	<100	<100	<100	<100	<100	<100	<100	<100	<100	<100
Q23_17	<100	<100	<100	<100	<100	116	383	165	369	427	197	635	260	1397	6536

Figure 6. Immunogenicity of MT145-WT Compared to MT145K Trimers in CH01 UCA HC-Only Knockin Mice

(A) Schematic showing immunization schedule of CH01 UCA HC-only KI mice with MT145-WT and engineered MT145K trimers. The CH01 UCA HC-only KI mice were immunized twice with 25 μg of the soluble trimer with glucopyranosyl lipid adjuvant stable emulsion (GLA-SE) as adjuvant. Time points for immunization and bleeds are indicated.

(B) ELISA binding of the MT145-WT and MT145K group trimer-immunized CH01 UCA HC-only KI mice serum samples (pre-bleed, Pre; 2 weeks post prime, Bleed #1; and 2 weeks post boost-1, Bleed #2) with soluble MT145K SOSIP and its glycan knockout variant (MT145K N160K) trimers.

(C) Neutralization titrations of the MT145-WT and MT145K group trimer immunized CH01 UCA HC-only KI mice sera (pre-bleed, Pre; post prime, Bleed #1; and post boost-1, Bleed #2) with MT145K virus and a CH01-sensitive virus (Q23_17). The 3-fold diluted sera were tested against the viruses in a TZM-bl reporter cell assay.

(D) The ID_{50} neutralization titers of the MT145-WT and MT145K group trimer-immunized CH01 UCA HC-only KI mice sera (pre- and post-immunization bleed time points). Neutralization was assessed against the priming immunogen-matched autologous viruses in each group (MT145-WT group, MT145-WT virus; MT145K group, MT145K virus), the N160 glycan knockout variant of the MT145K virus (MT145K N160A), and a highly CH01-sensitive virus, Q23_17. The numerical values shown in the table represent the ID_{50} neutralization titers of the immune serum samples and were calculated by non-linear regression method from the percent neutralizations of serum titrations with virus.

with the MT145K trimer, in the CH01 UCA KI mice. We further boosted the MT145K trimer immunized CH01 KI mice with a three-trimer cocktail (C108, WITO, and ZM197-ZM233V1V2 SOSIPs) (Figure 7A), derived from HIV subtype AG, B, and C viral isolates previously shown to be sensitive to CH01 bnAb lineage (Andrabi et al., 2015; Bonsignori et al., 2011; Gorman et al., 2016). Following boosting with the HIV trimer cocktail, the week-10 serum Ab responses (Bleed #4: 2-weeks post HIV trimer cocktail boosting) displayed cross-neutralizing activities against a panel of CH01-class bnAb sensitive heterologous HIV isolates (Figure 7B; Table S2). The serum Ab responses mapped entirely to the V2-apex bnAb epitope (Table S2), suggesting a successful nAb recall response to the V2-bnAb site upon HIV trimer boosting. Notably, the MT145K trimer prime

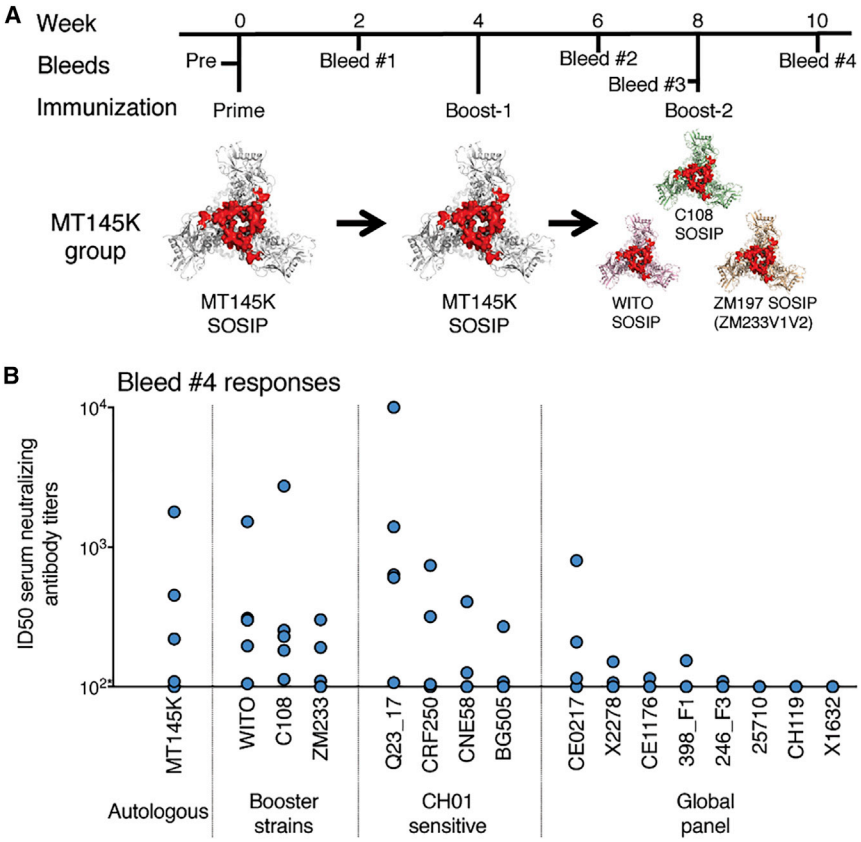

Figure 7. Boosting Chimpanzee SIV MT145K Trimer-Induced B Cell Responses with an HIV Trimer Cocktail in CH01 UCA HC-Only Knockin Mice

(A) Schematic showing immunization schedule of CH01 UCA HC-only KI mice with a chimpanzee SIV MT145K trimer followed by an HIV Env-derived three-trimer cocktail. A group of five animals was immunized with two doses (prime, week 0; boost-1, week 4) of the MT145K trimer (as also shown in Figure 6). The animals were further boosted (boost-2 at week 8) with an HIV Env-derived three-trimer cocktail (C108, WITO, and ZM197-ZM233V1V2). The V1V2 loops on trimer cartoons are depicted in red to highlight that the region is shared between HIV and SIV Env trimers. The CH01 UCA HC-only KI mice were immunized with 25 μg of the soluble MT145K trimer or HIV three-trimer cocktail (25 μg total) with GLA-SE as adjuvant. Time points for the immunizations and the bleeds are indicated.

(B) The ID50 virus neutralization titers of the Bleed #4 serum samples collected post boost-2 immunization with an HIV three-trimer cocktail. The neutralization of the post-immune sera was assessed against the priming immunogen-matched autologous virus, MT145K, the boosting immunogen-matched, CH01 sensitive viruses, and global panel HIV Env-encoding viruses. Each filled circle in the plot represents virus ID50 neutralization values for the individual animals; an asterisk (*) indicates that 50% neutralization was not reached at a 1:100 serum dilution.

boosting itself led to the development of sporadic cross-neutralizing responses against a few CH01-class bnAb sensitive HIV isolates (Bonsignori et al., 2011) (Table S2). However, HIV trimer boosting slightly improved further the neutralization breadth against heterologous viruses (Table S2), suggesting that the boosting immunizations resulted in the development of B cell responses along favorable pathways.

Interestingly, the trimer-elicited serum Ab responses in the CH01 UCA KI model mapped entirely to the glycan N160, as probed by ELISA binding with MT145K, CRF250 trimers, and their N160-glycan-eliminated trimer variants (Figure S9). The animals, however, did not develop Env backbone-specific off-target B cell responses at any stages of the SIV MT145K or HIV trimer immunizations. This result suggests that the very high frequency of CH01 UCA precursor B cells in the mouse model favors V2-apex responses to the exclusion of off-target responses. Therefore, this model was ultimately found to be unsuitable for evaluation of the advantages of a combined HIV and SIV immunization strategy and an adoptive transfer approach that can generate inter-epitope B cell clonal competition (Abbott et al., 2018; Dosenovic et al., 2018) may be more revealing.

Overall, the analysis of the immune responses revealed that, due to the extraordinary conservation of the V2-apex bnAb epitope region between HIV and chimpanzee SIV, the MT145K trimer successfully primed human V2-apex bnAb UCA-encoding mouse B cells and induced a V2-focused cross-neutralizing HIV Env-specific response that could be further boosted by HIV Env-derived trimers.

DISCUSSION

Vaccination has taken advantage of related viruses from different species, beginning with the use of cowpox as a smallpox vaccine (Riedel, 2005). HIV is too variable and has too many evasion mechanisms for such an approach applied directly to work effectively. Nevertheless, there are HIV-related viruses that have the potential to be exploited in some form in vaccine design. Indeed, the HIV pandemic is believed to have arisen because of a cross-species virus transmission from chimpanzees to humans during the period from 1910 to 1930 (Korber et al., 2000; Sharp and Hahn, 2011; Worobey et al., 2008). The HIV and chimpanzee SIV Envs, the target of potentially protective neutralizing antibodies, display about 60% sequence conservation at the amino-acid level. Importantly, HIV V2-apex bnAbs have been shown to neutralize certain chimpanzee SIV isolates, including the SIVcpz*Ptt* isolate MT145, suggesting cross-species conservation of this epitope (Barbian et al., 2015). Accordingly, we generated a chimpanzee SIV Env trimer (MT145 SOSIP) and showed that it bound HIV V2-apex bnAbs. We then engineered it to bind to germline-reverted V2-apex bnAbs (MT145K SOSIP) so that it might be useful in activating V2-apex precursors.

The cryo-EM structure of MT145K SOSIP trimer revealed that the Env trimers of HIV and chimpanzee SIV have very similar

overall architectures. The glycan shield of chimpanzee SIV forms a similarly dense protective layer to antibody recognition of the protein surface as observed in HIV. However, subtle movements in the locations of the glycans appear to contribute to the inability of the great majority of HIV bnAbs to recognize the chimpanzee SIV Env trimer. As noted above, bnAbs to the V2-apex region of the trimer are the exception. We have hypothesized previously (Lee et al., 2017) that the conservation of this region among HIV isolates is to facilitate trimer disassembly during viral entry. It is interesting that the overall V2-apex structure is conserved across the chimpanzee-human species barrier, indicating its critical importance for Env function.

In order to evaluate the MT145K trimer as an immunogen able to activate V2-apex bnAb precursor B cells, we took advantage of the availability of V2-apex bnAb UCA H-chain-only knockin mice. We compared MT145K and MT145 trimers as immunogens. Following two immunizations, MT145K trimers reproducibly elicited Abs able to neutralize the autologous virus and a few V2-apex Ab-sensitive viruses whereas MT145 trimers failed to induce such nAbs. The specificities of the nAbs were dependent on the glycan at N160 and a lysine on strand C of the V2. Boosting with a cocktail of HIV Env trimers successfully recalled the V2-apex-specific nAb responses and generated some enhanced heterologous neutralization. Therefore, from studies in this mouse model, the MT145K trimer appears to be a promising immunogen to induce V2-apex bnAbs. However, further immune evaluation of MT145K vaccine strategies in animal models expressing bnAb-encoding B cell precursors at frequencies closer to those expected in humans will be important (Abbott et al., 2018; Lee et al., 2014; Osborn et al., 2013).

STAR★METHODS

Detailed methods are provided in the online version of this paper and include the following:

SUPPLEMENTAL INFORMATION

Supplemental Information can be found online at https://doi.org/10.1016/j.celrep.2019.04.082.

ACKNOWLEDGMENTS

This work was supported by the International AIDS Vaccine Initiative (IAVI) through the Neutralizing Antibody Consortium SFP1849 (D.R.B., A.B.W., I.A.W., and M.C.), the National Institute of Allergy and Infectious Diseases (Center for HIV/AIDS Vaccine Immunology and Immunogen Discovery grant UM1AI100663 to D.R.B., A.B.W., I.A.W., and M.C.), and the Ragon Institute of MGH, MIT, and Harvard (D.R.B.). This study was made possible by the generous support of the Bill and Melinda Gates Foundation Collaboration for AIDS Vaccine Discovery (CAVD; OPP115782 and OPP1084519) and the American people through USAID. We thank Christina Corbaci and for her help in the preparation of the figures.

AUTHOR CONTRIBUTIONS

R.A., J.P., J.D.A., J.Z., L.V., A.B.W., and D.R.B. designed the experiments. R.A., J.P., J.D.A., G.S., J.Z., N.d.V., G.G., K.P., C.-Y.S., M.P., A.N., and F.G. performed the experiments. H.B.V., I.A.W., M.C., B.H.H., and B.F.H. contributed critical reagents. R.A., J.P., J.D.A., A.B.W., and D.R.B. analyzed the data and wrote the paper, with inputs from other authors. R.A. and D.R.B. conceived the idea of using SIVcpz*Ptt* Env-derived trimer as an HIV vaccine template.

DECLARATION OF INTERESTS

R.A. and D.R.B. are inventors on a patent application filed by International AIDS Vaccine Initiative (IAVI) and The Scripps Research Institute (TSRI) related to the data presented in this work. All other authors declare no competing interests.

Received: September 24, 2018
Revised: February 25, 2019
Accepted: April 17, 2019
Published: May 21, 2019

REFERENCES

Abbott, R.K., Lee, J.H., Menis, S., Skog, P., Rossi, M., Ota, T., Kulp, D.W., Bhullar, D., Kalyuzhniy, O., Havenar-Daughton, C., et al. (2018). Precursor Frequency and Affinity Determine B Cell Competitive Fitness in Germinal Centers, Tested with Germline-Targeting HIV Vaccine Immunogens. Immunity *48*, 133–146.e6.

Adams, P.D., Grosse-Kunstleve, R.W., Hung, L.W., Ioerger, T.R., McCoy, A.J., Moriarty, N.W., Read, R.J., Sacchettini, J.C., Sauter, N.K., and Terwilliger, T.C. (2002). PHENIX: building new software for automated crystallographic structure determination. Acta Crystallogr. D Biol. Crystallogr. *58*, 1948–1954.

Agirre, J., Iglesias-Fernández, J., Rovira, C., Davies, G.J., Wilson, K.S., and Cowtan, K.D. (2015). Privateer: software for the conformational validation of carbohydrate structures. Nat. Struct. Mol. Biol. *22*, 833–834.

Andrabi, R., Voss, J.E., Liang, C.H., Briney, B., McCoy, L.E., Wu, C.Y., Wong, C.H., Poignard, P., and Burton, D.R. (2015). Identification of Common Features in Prototype Broadly Neutralizing Antibodies to HIV Envelope V2 Apex to Facilitate Vaccine Design. Immunity *43*, 959–973.

Andrabi, R., Su, C.Y., Liang, C.H., Shivatare, S.S., Briney, B., Voss, J.E., Nawazi, S.K., Wu, C.Y., Wong, C.H., and Burton, D.R. (2017). Glycans Function as Anchors for Antibodies and Help Drive HIV Broadly Neutralizing Antibody Development. Immunity *47*, 524–537.e3.

Andrabi, R., Bhiman, J.N., and Burton, D.R. (2018). Strategies for a multi-stage neutralizing antibody-based HIV vaccine. Curr. Opin. Immunol. *53*, 143–151.

Barad, B.A., Echols, N., Wang, R.Y., Cheng, Y., DiMaio, F., Adams, P.D., and Fraser, J.S. (2015). EMRinger: side chain-directed model and map validation for 3D cryo-electron microscopy. Nat. Methods *12*, 943–946.

Barbian, H.J., Decker, J.M., Bibollet-Ruche, F., Galimidi, R.P., West, A.P., Jr., Learn, G.H., Parrish, N.F., Iyer, S.S., Li, Y., Pace, C.S., et al. (2015). Neutralization properties of simian immunodeficiency viruses infecting chimpanzees and gorillas. MBio *6*, e00296-15.

Behrens, A.J., Vasiljevic, S., Pritchard, L.K., Harvey, D.J., Andev, R.S., Krumm, S.A., Struwe, W.B., Cupo, A., Kumar, A., Zitzmann, N., et al. (2016). Composition and Antigenic Effects of Individual Glycan Sites of a Trimeric HIV-1 Envelope Glycoprotein. Cell Rep. *14*, 2695–2706.

Behrens, A.J., Harvey, D.J., Milne, E., Cupo, A., Kumar, A., Zitzmann, N., Struwe, W.B., Moore, J.P., and Crispin, M. (2017). Molecular Architecture of the Cleavage-Dependent Mannose Patch on a Soluble HIV-1 Envelope Glycoprotein Trimer. J. Virol. *91*, e01894-16.

Bhiman, J.N., Anthony, C., Doria-Rose, N.A., Karimanzira, O., Schramm, C.A., Khoza, T., Kitchin, D., Botha, G., Gorman, J., Garrett, N.J., et al. (2015). Viral variants that initiate and drive maturation of V1V2-directed HIV-1 broadly neutralizing antibodies. Nat. Med. *21*, 1332–1336.

Blattner, C., Lee, J.H., Sliepen, K., Derking, R., Falkowska, E., de la Peña, A.T., Cupo, A., Julien, J.P., van Gils, M., Lee, P.S., et al. (2014). Structural delineation of a quaternary, cleavage-dependent epitope at the gp41-gp120 interface on intact HIV-1 Env trimers. Immunity *40*, 669–680.

Bonomelli, C., Doores, K.J., Dunlop, D.C., Thaney, V., Dwek, R.A., Burton, D.R., Crispin, M., and Scanlan, C.N. (2011). The glycan shield of HIV is predominantly oligomannose independently of production system or viral clade. PLoS One *6*, e23521.

Bonsignori, M., Hwang, K.K., Chen, X., Tsao, C.Y., Morris, L., Gray, E., Marshall, D.J., Crump, J.A., Kapiga, S.H., Sam, N.E., et al. (2011). Analysis of a clonal lineage of HIV-1 envelope V2/V3 conformational epitope-specific broadly neutralizing antibodies and their inferred unmutated common ancestors. J. Virol. *85*, 9998–10009.

Braibant, M., Gong, E.Y., Plantier, J.C., Moreau, T., Alessandri, E., Simon, F., and Barin, F. (2013). Cross-group neutralization of HIV-1 and evidence for conservation of the PG9/PG16 epitopes within divergent groups. AIDS *27*, 1239–1244.

Briney, B.S., Willis, J.R., and Crowe, J.E., Jr. (2012). Human peripheral blood antibodies with long HCDR3s are established primarily at original recombination using a limited subset of germline genes. PLoS One *7*, e36750.

Briney, B., Sok, D., Jardine, J.G., Kulp, D.W., Skog, P., Menis, S., Jacak, R., Kalyuzhniy, O., de Val, N., Sesterhenn, F., et al. (2016). Tailored Immunogens Direct Affinity Maturation toward HIV Neutralizing Antibodies. Cell *166*, 1459–1470.e11.

Brochet, X., Lefranc, M.P., and Giudicelli, V. (2008). IMGT/V-QUEST: the highly customized and integrated system for IG and TR standardized V-J and V-D-J sequence analysis. Nucleic Acids Res. *36*, W503–W508.

Chen, V.B., Arendall, W.B., 3rd, Headd, J.J., Keedy, D.A., Immormino, R.M., Kapral, G.J., Murray, L.W., Richardson, J.S., and Richardson, D.C. (2010). MolProbity: all-atom structure validation for macromolecular crystallography. Acta Crystallogr. D Biol. Crystallogr. *66*, 12–21.

Chen, Y., Zhang, J., Hwang, K.K., Bouton-Verville, H., Xia, S.M., Newman, A., Ouyang, Y.B., Haynes, B.F., and Verkoczy, L. (2013). Common tolerance mechanisms, but distinct cross-reactivities associated with gp41 and lipids, limit production of HIV-1 broad neutralizing antibodies 2F5 and 4E10. J. Immunol. *191*, 1260–1275.

DiMaio, F., Song, Y., Li, X., Brunner, M.J., Xu, C., Conticello, V., Egelman, E., Marlovits, T., Cheng, Y., and Baker, D. (2015). Atomic-accuracy models from 4.5-Å cryo-electron microscopy data with density-guided iterative local refinement. Nat. Methods *12*, 361–365.

Doria-Rose, N.A., Schramm, C.A., Gorman, J., Moore, P.L., Bhiman, J.N., DeKosky, B.J., Ernandes, M.J., Georgiev, I.S., Kim, H.J., Pancera, M., et al.; NISC Comparative Sequencing Program (2014). Developmental pathway for potent V1V2-directed HIV-neutralizing antibodies. Nature *509*, 55–62.

Dosenovic, P., von Boehmer, L., Escolano, A., Jardine, J., Freund, N.T., Gitlin, A.D., McGuire, A.T., Kulp, D.W., Oliveira, T., Scharf, L., et al. (2015). Immunization for HIV-1 Broadly Neutralizing Antibodies in Human Ig Knockin Mice. Cell *161*, 1505–1515.

Dosenovic, P., Kara, E.E., Pettersson, A.K., McGuire, A.T., Gray, M., Hartweger, H., Thientosapol, E.S., Stamatatos, L., and Nussenzweig, M.C. (2018). Anti-HIV-1 B cell responses are dependent on B cell precursor frequency and antigen-binding affinity. Proc. Natl. Acad. Sci. USA *115*, 4743–4748.

Emsley, P., and Cowtan, K. (2004). Coot: model-building tools for molecular graphics. Acta Crystallogr. D Biol. Crystallogr. *60*, 2126–2132.

Escolano, A., Steichen, J.M., Dosenovic, P., Kulp, D.W., Golijanin, J., Sok, D., Freund, N.T., Gitlin, A.D., Oliveira, T., Araki, T., et al. (2016). Sequential Immunization Elicits Broadly Neutralizing Anti-HIV-1 Antibodies in Ig Knockin Mice. Cell *166*, 1445–1458.e12.

Escolano, A., Dosenovic, P., and Nussenzweig, M.C. (2017). Progress toward active or passive HIV-1 vaccination. J. Exp. Med. *214*, 3–16.

Falkowska, E., Le, K.M., Ramos, A., Doores, K.J., Lee, J.H., Blattner, C., Ramirez, A., Derking, R., van Gils, M.J., Liang, C.H., et al. (2014). Broadly neutralizing HIV antibodies define a glycan-dependent epitope on the prefusion conformation of gp41 on cleaved envelope trimers. Immunity *40*, 657–668.

Gao, F., Bailes, E., Robertson, D.L., Chen, Y., Rodenburg, C.M., Michael, S.F., Cummins, L.B., Arthur, L.O., Peeters, M., Shaw, G.M., et al. (1999). Origin of HIV-1 in the chimpanzee Pan troglodytes troglodytes. Nature *397*, 436–441.

Garces, F., Sok, D., Kong, L., McBride, R., Kim, H.J., Saye-Francisco, K.F., Julien, J.P., Hua, Y., Cupo, A., Moore, J.P., et al. (2014). Structural evolution of glycan recognition by a family of potent HIV antibodies. Cell *159*, 69–79.

Garces, F., Lee, J.H., de Val, N., de la Pena, A.T., Kong, L., Puchades, C., Hua, Y., Stanfield, R.L., Burton, D.R., Moore, J.P., et al. (2015). Affinity Maturation of a Potent Family of HIV Antibodies Is Primarily Focused on Accommodating or Avoiding Glycans. Immunity *43*, 1053–1063.

Georgiev, I.S., Doria-Rose, N.A., Zhou, T., Kwon, Y.D., Staupe, R.P., Moquin, S., Chuang, G.Y., Louder, M.K., Schmidt, S.D., Altae-Tran, H.R., et al. (2013). Delineating antibody recognition in polyclonal sera from patterns of HIV-1 isolate neutralization. Science *340*, 751–756.

Gorman, J., Soto, C., Yang, M.M., Davenport, T.M., Guttman, M., Bailer, R.T., Chambers, M., Chuang, G.Y., DeKosky, B.J., Doria-Rose, N.A., et al.; NISC Comparative Sequencing Program (2016). Structures of HIV-1 Env V1V2 with broadly neutralizing antibodies reveal commonalities that enable vaccine design. Nat. Struct. Mol. Biol. *23*, 81–90.

Gristick, H.B., von Boehmer, L., West, A.P., Jr., Schamber, M., Gazumyan, A., Golijanin, J., Seaman, M.S., Fätkenheuer, G., Klein, F., Nussenzweig, M.C., and Bjorkman, P.J. (2016). Natively glycosylated HIV-1 Env structure reveals new mode for antibody recognition of the CD4-binding site. Nat. Struct. Mol. Biol. *23*, 906–915.

Harvey, D.J., Baruah, K., and Scanlan, C.N. (2009). Application of negative ion MS/MS to the identification of N-glycans released from carcinoembryonic antigen cell adhesion molecule 1 (CEACAM1). J. Mass Spectrom. *44*, 50–60.

Havenar-Daughton, C., Lee, J.H., and Crotty, S. (2017). Tfh cells and HIV bnAbs, an immunodominance model of the HIV neutralizing antibody generation problem. Immunol. Rev. *275*, 49–61.

Haynes, B.F., and Mascola, J.R. (2017). The quest for an antibody-based HIV vaccine. Immunol. Rev. *275*, 5–10.

Haynes, B.F., Kelsoe, G., Harrison, S.C., and Kepler, T.B. (2012). B-cell-lineage immunogen design in vaccine development with HIV-1 as a case study. Nat. Biotechnol. *30*, 423–433.

Jardine, J., Julien, J.P., Menis, S., Ota, T., Kalyuzhniy, O., McGuire, A., Sok, D., Huang, P.S., MacPherson, S., Jones, M., et al. (2013). Rational HIV immunogen design to target specific germline B cell receptors. Science *340*, 711–716.

Jardine, J.G., Ota, T., Sok, D., Pauthner, M., Kulp, D.W., Kalyuzhniy, O., Skog, P.D., Thinnes, T.C., Bhullar, D., Briney, B., et al. (2015). HIV-1 VACCINES. Priming a broadly neutralizing antibody response to HIV-1 using a germline-targeting immunogen. Science *349*, 156–161.

Julien, J.P., Cupo, A., Sok, D., Stanfield, R.L., Lyumkis, D., Deller, M.C., Klasse, P.J., Burton, D.R., Sanders, R.W., Moore, J.P., et al. (2013a). Crystal structure of a soluble cleaved HIV-1 envelope trimer. Science *342*, 1477–1483.

Julien, J.P., Lee, J.H., Cupo, A., Murin, C.D., Derking, R., Hoffenberg, S., Caulfield, M.J., King, C.R., Marozsan, A.J., Klasse, P.J., et al. (2013b). Asymmetric recognition of the HIV-1 trimer by broadly neutralizing antibody PG9. Proc. Natl. Acad. Sci. USA *110*, 4351–4356.

Kepler, T.B., Liao, H.X., Alam, S.M., Bhaskarabhatla, R., Zhang, R., Yandava, C., Stewart, S., Anasti, K., Kelsoe, G., Parks, R., et al. (2014). Immunoglobulin gene insertions and deletions in the affinity maturation of HIV-1 broadly reactive neutralizing antibodies. Cell Host Microbe *16*, 304–313.

Klein, F., Diskin, R., Scheid, J.F., Gaebler, C., Mouquet, H., Georgiev, I.S., Pancera, M., Zhou, T., Incesu, R.B., Fu, B.Z., et al. (2013). Somatic mutations of the immunoglobulin framework are generally required for broad and potent HIV-1 neutralization. Cell *153*, 126–138.

Kong, L., Lee, J.H., Doores, K.J., Murin, C.D., Julien, J.P., McBride, R., Liu, Y., Marozsan, A., Cupo, A., Klasse, P.J., et al. (2013). Supersite of immune vulnerability on the glycosylated face of HIV-1 envelope glycoprotein gp120. Nat. Struct. Mol. Biol. *20*, 796–803.

Korber, B., Muldoon, M., Theiler, J., Gao, F., Gupta, R., Lapedes, A., Hahn, B.H., Wolinsky, S., and Bhattacharya, T. (2000). Timing the ancestor of the HIV-1 pandemic strains. Science *288*, 1789–1796.

Kwon, Y.D., Pancera, M., Acharya, P., Georgiev, I.S., Crooks, E.T., Gorman, J., Joyce, M.G., Guttman, M., Ma, X., Narpala, S., et al. (2015). Crystal structure, conformational fixation and entry-related interactions of mature ligand-free HIV-1 Env. Nat. Struct. Mol. Biol. *22*, 522–531.

Landais, E., Huang, X., Havenar-Daughton, C., Murrell, B., Price, M.A., Wickramasinghe, L., Ramos, A., Bian, C.B., Simek, M., Allen, S., et al. (2016). Broadly Neutralizing Antibody Responses in a Large Longitudinal Sub-Saharan HIV Primary Infection Cohort. PLoS Pathog. *12*, e1005369.

Landais, E., Murrell, B., Briney, B., Murrell, S., Rantalainen, K., Berndsen, Z.T., Ramos, A., Wickramasinghe, L., Smith, M.L., Eren, K., et al. (2017). HIV Envelope Glycoform Heterogeneity and Localized Diversity Govern the Initiation and Maturation of a V2 Apex Broadly Neutralizing Antibody Lineage. Immunity *47*, 990–1003.e9.

Lee, E.C., Liang, Q., Ali, H., Bayliss, L., Beasley, A., Bloomfield-Gerdes, T., Bonoli, L., Brown, R., Campbell, J., Carpenter, A., et al. (2014). Complete humanization of the mouse immunoglobulin loci enables efficient therapeutic antibody discovery. Nat. Biotechnol. *32*, 356–363.

Lee, J.H., de Val, N., Lyumkis, D., and Ward, A.B. (2015). Model Building and Refinement of a Natively Glycosylated HIV-1 Env Protein by High-Resolution Cryoelectron Microscopy. Structure *23*, 1943–1951.

Lee, J.H., Ozorowski, G., and Ward, A.B. (2016). Cryo-EM structure of a native, fully glycosylated, cleaved HIV-1 envelope trimer. Science *351*, 1043–1048.

Lee, J.H., Andrabi, R., Su, C.Y., Yasmeen, A., Julien, J.P., Kong, L., Wu, N.C., McBride, R., Sok, D., Pauthner, M., et al. (2017). A Broadly Neutralizing Antibody Targets the Dynamic HIV Envelope Trimer Apex via a Long, Rigidified, and Anionic β-Hairpin Structure. Immunity *46*, 690–702.

Lyumkis, D., Julien, J.P., de Val, N., Cupo, A., Potter, C.S., Klasse, P.J., Burton, D.R., Sanders, R.W., Moore, J.P., Carragher, B., et al. (2013). Cryo-EM structure of a fully glycosylated soluble cleaved HIV-1 envelope trimer. Science *342*, 1484–1490.

McCoy, L.E., Quigley, A.F., Strokappe, N.M., Bulmer-Thomas, B., Seaman, M.S., Mortier, D., Rutten, L., Chander, N., Edwards, C.J., Ketteler, R., et al. (2012). Potent and broad neutralization of HIV-1 by a llama antibody elicited by immunization. J. Exp. Med. *209*, 1091–1103.

McGuire, A.T., Hoot, S., Dreyer, A.M., Lippy, A., Stuart, A., Cohen, K.W., Jardine, J., Menis, S., Scheid, J.F., West, A.P., et al. (2013). Engineering HIV envelope protein to activate germline B cell receptors of broadly neutralizing anti-CD4 binding site antibodies. J. Exp. Med. *210*, 655–663.

McGuire, A.T., Gray, M.D., Dosenovic, P., Gitlin, A.D., Freund, N.T., Petersen, J., Correnti, C., Johnsen, W., Kegel, R., Stuart, A.B., et al. (2016). Specifically modified Env immunogens activate B-cell precursors of broadly neutralizing HIV-1 antibodies in transgenic mice. Nat. Commun. *7*, 10618.

McLellan, J.S., Pancera, M., Carrico, C., Gorman, J., Julien, J.P., Khayat, R., Louder, R., Pejchal, R., Sastry, M., Dai, K., et al. (2011). Structure of HIV-1 gp120 V1/V2 domain with broadly neutralizing antibody PG9. Nature *480*, 336–343.

McLellan, J.S., Chen, M., Leung, S., Graepel, K.W., Du, X., Yang, Y., Zhou, T., Baxa, U., Yasuda, E., Beaumont, T., et al. (2013). Structure of RSV fusion glycoprotein trimer bound to a prefusion-specific neutralizing antibody. Science *340*, 1113–1117.

Montefiori, D.C. (2005). Evaluating neutralizing antibodies against HIV, SIV, and SHIV in luciferase reporter gene assays. Curr. Protoc. Immunol. *Chapter 12*, Unit 12.11.

Moore, P.L., Gray, E.S., Sheward, D., Madiga, M., Ranchobe, N., Lai, Z., Honnen, W.J., Nonyane, M., Tumba, N., Hermanus, T., et al.; CAPRISA 002 Study (2011). Potent and broad neutralization of HIV-1 subtype C by plasma antibodies targeting a quaternary epitope including residues in the V2 loop. J. Virol. *85*, 3128–3141.

Moore, P.L., Gorman, J., Doria-Rose, N.A., and Morris, L. (2017). Ontogeny-based immunogens for the induction of V2-directed HIV broadly neutralizing antibodies. Immunol. Rev. *275*, 217–229.

Morgand, M., Bouvin-Pley, M., Plantier, J.C., Moreau, A., Alessandri, E., Simon, F., Pace, C.S., Pancera, M., Ho, D.D., Poignard, P., et al. (2016). V1/V2 Neutralizing Epitope is Conserved in Divergent Non-M Groups of HIV-1. J. Acquir. Immune Defic. Syndr. *71*, 237–245.

Ogura, T., Iwasaki, K., and Sato, C. (2003). Topology representing network enables highly accurate classification of protein images taken by cryo electron-microscope without masking. J. Struct. Biol. *143*, 185–200.

Osborn, M.J., Ma, B., Avis, S., Binnie, A., Dilley, J., Yang, X., Lindquist, K., Ménoret, S., Iscache, A.L., Ouisse, L.H., et al. (2013). High-affinity IgG antibodies develop naturally in Ig-knockout rats carrying germline human IgH/Igκ/Igλ loci bearing the rat CH region. J. Immunol. *190*, 1481–1490.

Ozorowski, G., Pallesen, J., de Val, N., Lyumkis, D., Cottrell, C.A., Torres, J.L., Copps, J., Stanfield, R.L., Cupo, A., Pugach, P., et al. (2017). Open and closed structures reveal allostery and pliability in the HIV-1 envelope spike. Nature *547*, 360–363.

Pallesen, J., Murin, C.D., de Val, N., Cottrell, C.A., Hastie, K.M., Turner, H.L., Fusco, M.L., Flyak, A.I., Zeitlin, L., Crowe, J.E., Jr., et al. (2016). Structures of Ebola virus GP and sGP in complex with therapeutic antibodies. Nat. Microbiol. *1*, 16128.

Pallesen, J., Wang, N., Corbett, K.S., Wrapp, D., Kirchdoerfer, R.N., Turner, H.L., Cottrell, C.A., Becker, M.M., Wang, L., Shi, W., et al. (2017). Immunogenicity and structures of a rationally designed prefusion MERS-CoV spike antigen. Proc. Natl. Acad. Sci. USA *114*, E7348–E7357.

Pancera, M., Shahzad-Ul-Hussan, S., Doria-Rose, N.A., McLellan, J.S., Bailer, R.T., Dai, K., Loesgen, S., Louder, M.K., Staupe, R.P., Yang, Y., et al. (2013). Structural basis for diverse N-glycan recognition by HIV-1-neutralizing V1-V2-directed antibody PG16. Nat. Struct. Mol. Biol. *20*, 804–813.

Pancera, M., Zhou, T., Druz, A., Georgiev, I.S., Soto, C., Gorman, J., Huang, J., Acharya, P., Chuang, G.Y., Ofek, G., et al. (2014). Structure and immune recognition of trimeric pre-fusion HIV-1 Env. Nature *514*, 455–461.

Panico, M., Bouché, L., Binet, D., O'Connor, M.J., Rahman, D., Pang, P.C., Canis, K., North, S.J., Desrosiers, R.C., Chertova, E., et al. (2016). Mapping the complete glycoproteome of virion-derived HIV-1 gp120 provides insights into broadly neutralizing antibody binding. Sci. Rep. *6*, 32956.

Pejchal, R., Doores, K.J., Walker, L.M., Khayat, R., Huang, P.S., Wang, S.K., Stanfield, R.L., Julien, J.P., Ramos, A., Crispin, M., et al. (2011). A potent and broad neutralizing antibody recognizes and penetrates the HIV glycan shield. Science *334*, 1097–1103.

Pettersen, E.F., Goddard, T.D., Huang, C.C., Couch, G.S., Greenblatt, D.M., Meng, E.C., and Ferrin, T.E. (2004). UCSF Chimera–a visualization system for exploratory research and analysis. J. Comput. Chem. *25*, 1605–1612.

Pritchard, L.K., Harvey, D.J., Bonomelli, C., Crispin, M., and Doores, K.J. (2015). Cell- and Protein-Directed Glycosylation of Native Cleaved HIV-1 Envelope. J. Virol. *89*, 8932–8944.

Pugach, P., Ozorowski, G., Cupo, A., Ringe, R., Yasmeen, A., de Val, N., Derking, R., Kim, H.J., Korzun, J., Golabek, M., et al. (2015). A native-like SOSIP.664 trimer based on an HIV-1 subtype B env gene. J. Virol. *89*, 3380–3395.

Riedel, S. (2005). Edward Jenner and the history of smallpox and vaccination. Proc. Bayl. Univ. Med. Cent. *18*, 21–25.

Sanders, R.W., Derking, R., Cupo, A., Julien, J.P., Yasmeen, A., de Val, N., Kim, H.J., Blattner, C., de la Peña, A.T., Korzun, J., et al. (2013). A next-generation cleaved, soluble HIV-1 Env trimer, BG505 SOSIP.664 gp140, expresses multiple epitopes for broadly neutralizing but not non-neutralizing antibodies. PLoS Pathog. *9*, e1003618.

Sanders, R.W., van Gils, M.J., Derking, R., Sok, D., Ketas, T.J., Burger, J.A., Ozorowski, G., Cupo, A., Simonich, C., Goo, L., et al. (2015). HIV-1 VACCINES. HIV-1 neutralizing antibodies induced by native-like envelope trimers. Science *349*, aac4223.

Saunders, K.O., Verkoczy, L.K., Jiang, C., Zhang, J., Parks, R., Chen, H., Housman, M., Bouton-Verville, H., Shen, X., Trama, A.M., et al. (2017). Vaccine Induction of Heterologous Tier 2 HIV-1 Neutralizing Antibodies in Animal Models. Cell Rep. *21*, 3681–3690.

Scheres, S.H. (2012). RELION: implementation of a Bayesian approach to cryo-EM structure determination. J. Struct. Biol. *180*, 519–530.

Seaman, M.S., Janes, H., Hawkins, N., Grandpre, L.E., Devoy, C., Giri, A., Coffey, R.T., Harris, L., Wood, B., Daniels, M.G., et al. (2010). Tiered categorization of a diverse panel of HIV-1 Env pseudoviruses for assessment of neutralizing antibodies. J. Virol. *84*, 1439–1452.

Sharma, S.K., de Val, N., Bale, S., Guenaga, J., Tran, K., Feng, Y., Dubrovskaya, V., Ward, A.B., and Wyatt, R.T. (2015). Cleavage-independent HIV-1 Env trimers engineered as soluble native spike mimetics for vaccine design. Cell Rep. *11*, 539–550.

Sharp, P.M., and Hahn, B.H. (2011). Origins of HIV and the AIDS pandemic. Cold Spring Harb. Perspect. Med. *1*, a006841.

Sok, D., Doores, K.J., Briney, B., Le, K.M., Saye-Francisco, K.L., Ramos, A., Kulp, D.W., Julien, J.P., Menis, S., Wickramasinghe, L., et al. (2014a). Promiscuous glycan site recognition by antibodies to the high-mannose patch of gp120 broadens neutralization of HIV. Sci. Transl. Med. *6*, 236ra63.

Sok, D., van Gils, M.J., Pauthner, M., Julien, J.P., Saye-Francisco, K.L., Hsueh, J., Briney, B., Lee, J.H., Le, K.M., Lee, P.S., et al. (2014b). Recombinant HIV envelope trimer selects for quaternary-dependent antibodies targeting the trimer apex. Proc. Natl. Acad. Sci. USA *111*, 17624–17629.

Sok, D., Briney, B., Jardine, J.G., Kulp, D.W., Menis, S., Pauthner, M., Wood, A., Lee, E.C., Le, K.M., Jones, M., et al. (2016a). Priming HIV-1 broadly neutralizing antibody precursors in human Ig loci transgenic mice. Science *353*, 1557–1560.

Sok, D., Pauthner, M., Briney, B., Lee, J.H., Saye-Francisco, K.L., Hsueh, J., Ramos, A., Le, K.M., Jones, M., Jardine, J.G., et al. (2016b). A Prominent Site of Antibody Vulnerability on HIV Envelope Incorporates a Motif Associated with CCR5 Binding and Its Camouflaging Glycans. Immunity *45*, 31–45.

Sok, D., Le, K.M., Vadnais, M., Saye-Francisco, K.L., Jardine, J.G., Torres, J.L., Berndsen, Z.T., Kong, L., Stanfield, R., Ruiz, J., et al. (2017). Rapid elicitation of broadly neutralizing antibodies to HIV by immunization in cows. Nature *548*, 108–111.

Steichen, J.M., Kulp, D.W., Tokatlian, T., Escolano, A., Dosenovic, P., Stanfield, R.L., McCoy, L.E., Ozorowski, G., Hu, X., Kalyuzhniy, O., et al. (2016). HIV Vaccine Design to Target Germline Precursors of Glycan-Dependent Broadly Neutralizing Antibodies. Immunity *45*, 483–496.

Stevens, J., Corper, A.L., Basler, C.F., Taubenberger, J.K., Palese, P., and Wilson, I.A. (2004). Structure of the uncleaved human H1 hemagglutinin from the extinct 1918 influenza virus. Science *303*, 1866–1870.

Tas, J.M., Mesin, L., Pasqual, G., Targ, S., Jacobsen, J.T., Mano, Y.M., Chen, C.S., Weill, J.C., Reynaud, C.A., Browne, E.P., et al. (2016). Visualizing antibody affinity maturation in germinal centers. Science *351*, 1048–1054.

Tian, M., Cheng, C., Chen, X., Duan, H., Cheng, H.L., Dao, M., Sheng, Z., Kimble, M., Wang, L., Lin, S., et al. (2016). Induction of HIV Neutralizing Antibody Lineages in Mice with Diverse Precursor Repertoires. Cell *166*, 1471–1484.e18.

Tiller, T., Meffre, E., Yurasov, S., Tsuiji, M., Nussenzweig, M.C., and Wardemann, H. (2008). Efficient generation of monoclonal antibodies from single human B cells by single cell RT-PCR and expression vector cloning. J. Immunol. Methods *329*, 112–124.

Verkoczy, L., Diaz, M., Holl, T.M., Ouyang, Y.B., Bouton-Verville, H., Alam, S.M., Liao, H.X., Kelsoe, G., and Haynes, B.F. (2010). Autoreactivity in an HIV-1 broadly reactive neutralizing antibody variable region heavy chain induces immunologic tolerance. Proc. Natl. Acad. Sci. USA *107*, 181–186.

Verkoczy, L., Chen, Y., Bouton-Verville, H., Zhang, J., Diaz, M., Hutchinson, J., Ouyang, Y.B., Alam, S.M., Holl, T.M., Hwang, K.K., et al. (2011). Rescue of HIV-1 broad neutralizing antibody-expressing B cells in 2F5 VH x VL knockin mice reveals multiple tolerance controls. J. Immunol. *187*, 3785–3797.

Voss, J.E., Andrabi, R., McCoy, L.E., de Val, N., Fuller, R.P., Messmer, T., Su, C.Y., Sok, D., Khan, S.N., Garces, F., et al. (2017). Elicitation of Neutralizing Antibodies Targeting the V2 Apex of the HIV Envelope Trimer in a Wild-Type Animal Model. Cell Rep. *21*, 222–235.

Voss, N.R., Yoshioka, C.K., Radermacher, M., Potter, C.S., and Carragher, B. (2009). DoG Picker and TiltPicker: software tools to facilitate particle selection in single particle electron microscopy. J. Struct. Biol. *166*, 205–213.

Walker, L.M., Phogat, S.K., Chan-Hui, P.Y., Wagner, D., Phung, P., Goss, J.L., Wrin, T., Simek, M.D., Fling, S., Mitcham, J.L., et al.; Protocol G Principal Investigators (2009). Broad and potent neutralizing antibodies from an African donor reveal a new HIV-1 vaccine target. Science *326*, 285–289.

Walker, L.M., Huber, M., Doores, K.J., Falkowska, E., Pejchal, R., Julien, J.P., Wang, S.K., Ramos, A., Chan-Hui, P.Y., Moyle, M., et al.; Protocol G Principal Investigators (2011). Broad neutralization coverage of HIV by multiple highly potent antibodies. Nature *477*, 466–470.

Wang, S., Mata-Fink, J., Kriegsman, B., Hanson, M., Irvine, D.J., Eisen, H.N., Burton, D.R., Wittrup, K.D., Kardar, M., and Chakraborty, A.K. (2015). Manipulating the selection forces during affinity maturation to generate cross-reactive HIV antibodies. Cell *160*, 785–797.

Webb, B., and Sali, A. (2016). Comparative Protein Structure Modeling Using MODELLER. Curr. Protoc. Bioinformatics *Chapter 5*, Unit-5.6.

Wibmer, C.K., Bhiman, J.N., Gray, E.S., Tumba, N., Abdool Karim, S.S., Williamson, C., Morris, L., and Moore, P.L. (2013). Viral escape from HIV-1 neutralizing antibodies drives increased plasma neutralization breadth through sequential recognition of multiple epitopes and immunotypes. PLoS Pathog. *9*, e1003738.

Williams, W.B., Zhang, J., Jiang, C., Nicely, N.I., Fera, D., Luo, K., Moody, M.A., Liao, H.X., Alam, S.M., Kepler, T.B., et al. (2017). Initiation of HIV neutralizing B cell lineages with sequential envelope immunizations. Nat. Commun. *8*, 1732.

Worobey, M., Gemmel, M., Teuwen, D.E., Haselkorn, T., Kunstman, K., Bunce, M., Muyembe, J.J., Kabongo, J.M., Kalengayi, R.M., Van Marck, E., et al. (2008). Direct evidence of extensive diversity of HIV-1 in Kinshasa by 1960. Nature *455*, 661–664.

Wu, X., Yang, Z.Y., Li, Y., Hogerkorp, C.M., Schief, W.R., Seaman, M.S., Zhou, T., Schmidt, S.D., Wu, L., Xu, L., et al. (2010). Rational design of envelope identifies broadly neutralizing human monoclonal antibodies to HIV-1. Science *329*, 856–861.

Xiao, X., Chen, W., Feng, Y., Zhu, Z., Prabakaran, P., Wang, Y., Zhang, M.Y., Longo, N.S., and Dimitrov, D.S. (2009). Germline-like predecessors of broadly neutralizing antibodies lack measurable binding to HIV-1 envelope glycoproteins: implications for evasion of immune responses and design of vaccine immunogens. Biochem. Biophys. Res. Commun. *390*, 404–409.

Xu, K., Acharya, P., Kong, R., Cheng, C., Chuang, G.Y., Liu, K., Louder, M.K., O'Dell, S., Rawi, R., Sastry, M., et al. (2018). Epitope-based vaccine design yields fusion peptide-directed antibodies that neutralize diverse strains of HIV-1. Nat. Med. *24*, 857–867.

Zhang, K. (2016). Gctf: Real-time CTF determination and correction. J. Struct. Biol. *193*, 1–12.

Zhang, M., Gaschen, B., Blay, W., Foley, B., Haigwood, N., Kuiken, C., and Korber, B. (2004). Tracking global patterns of N-linked glycosylation site variation in highly variable viral glycoproteins: HIV, SIV, and HCV envelopes and influenza hemagglutinin. Glycobiology *14*, 1229–1246.

Zheng, S.Q., Palovcak, E., Armache, J.P., Verba, K.A., Cheng, Y., and Agard, D.A. (2017). MotionCor2: anisotropic correction of beam-induced motion for improved cryo-electron microscopy. Nat. Methods *14*, 331–332.

Zhou, T., Georgiev, I., Wu, X., Yang, Z.Y., Dai, K., Finzi, A., Kwon, Y.D., Scheid, J.F., Shi, W., Xu, L., et al. (2010). Structural basis for broad and potent neutralization of HIV-1 by antibody VRC01. Science *329*, 811–817.

STAR★METHODS

KEY RESOURCES TABLE

REAGENT or RESOURCE	SOURCE	IDENTIFIER
Antibodies		
Monoclonal anti-HIV-1 Env PGT145	Produced in house; Walker et al., 2011	NA
Monoclonal anti-HIV-1 Env PG9	Produced in house; Walker et al., 2009	NA
Monoclonal anti-HIV-1 Env PG9 iGL	Produced in house; This paper	N/A
Monoclonal anti-HIV-1 Env CAP256.09	Produced in house; Doria-Rose et al., 2014	N/A
Monoclonal anti-HIV-1 Env CAP256 UCA	produced in house; Doria-Rose et al., 2014	N/A
Monoclonal anti-HIV-1 Env CH01	Produced in house; Bonsignori et al., 2011	N/A
Monoclonal anti-HIV-1 Env CH01 iGL	Produced in house; This paper	N/A
HIV mAbs	NIH AIDS Reagent Program or various research laboratories	N/A
Alkaline Phosphatase-AffiniPure Goat Anti-Human IgG, Fc Fragment Specific	Fisher Scientific	Cat# 109-055-098
Bacterial and Virus Strains		
BG505_W6M_C2	NIH AIDS Reagent Program	N/A
MT145K	This paper	N/A
Q23_17	NIH AIDS Reagent Program	N/A
WITO4160_33	NIH AIDS Reagent Program	N/A
C1080_C3	NIH AIDS Reagent Program	N/A
ZM233_6	NIH AIDS Reagent Program	N/A
12 virus panel – global isolates	NIH AIDS Reagent Program	N/A
Chemicals, Peptides, and Recombinant Proteins		
X-tremeGENE 9 DNA Transfection Reagent	Sigma-Aldrich	Cat# 6365809001
PEI MAX 40000	Polysciences, Inc.	Cat# 24765-1
Galanthus nivalis lectin (snow drop),agarose bound	Vector Labs	Cat#AL-1243
DEAE-Dextran	Sigma-Aldrich	Cat# D9885-10G
GAB1 SOSIP.664	This paper	N/A
MB897 SOSIP.664	This paper	N/A
EK505 SOSIP.664	This paper	N/A
MT145 SOSIP.664	This paper	N/A
MT145K SOSIP.664	This paper	N/A
Critical Commercial Assays		
QuikChange II XL Site-Directed Mutagenesis Kit	Agilent Technologies	Cat# 200522
Bright-Glo Luciferase Assay System	Promega	Cat# E2610
Deposited Data		
MT145K structure	This study	EMDB # EMD-20074 PDB # 6OHY
Experimental Models: Cell Lines		
HEK293T	ATCC	Cat# CRL-3216
FreeStyle 293-F	Thermo Fisher Scientific	Cat# R79007
TZM-bl cells	NIH AIDS Reagent Program	Cat# 8129
Experimental Models: Organisms/Strains		
CH01 UCA HC-only knock-in mouse model	This study	NA
Recombinant DNA		
pSG3Δenv plasmid	NIH AIDS Reagent Program	Cat# 11051

(*Continued on next page*)

Continued

REAGENT or RESOURCE	SOURCE	IDENTIFIER
Software and Algorithms		
Prism v7.0	GraphPad	https://www.graphpad.com/scientific-software/prism/
UCSF Chimera	Pettersen et al., 2004	N/A
Other		
Superdex 200 Increase 10/300 GL column	GE Healthcare	Cat# 28990944
Anti-human IgG Fc Capture (AHC) Biosensors	ForteBio	Cat#18-5060
Titan Krios	Thermo Fisher Scientific	N/A
K2 Summit	Gatan	N/A
Motioncor2	Zheng et al., 2017	N/A
GCTF	Zhang, 2016	N/A
Relion	Scheres, 2012	N/A
Rosetta	Rosetta Commons	https://www.rosettacommons.org/
Coot	Emsley and Cowtan, 2004	N/A

CONTACT FOR REAGENT AND RESOURCE SHARING

Further information and requests for resources and reagents should be directed to and will be fulfilled by the Lead Contact, Dennis R. Burton (burton@scripps.edu).

EXPERIMENTAL MODEL AND SUBJECT DETAILS

Knockin Mice

"CH01 UCA homozygous "HC only" ($V_HDJ_H^{+/+}$) site-directed transgenic, i.e., knock-in (KI) mice, with homozygously knocked-in CH01 UCA V_HDJ_H rearrangements, were generated on the C57BL/6 background based on previously-described IgH locus-directed gene-targeting techniques (Chen et al., 2013; Verkoczy et al., 2011; Verkoczy et al., 2010). All vaccinations were performed using 6-12-week-old mice, and all immunization groups were equally matched for gender. All mice were cared for in a facility accredited by the Association for Assessment and Accreditation of Laboratory Animal Care International (AAALAC), in accordance with NIH guidelines. All animal procedures were approved by the Duke Institutional Animal Care and Use Committee (IACUC), prior to performance.

Cell Lines

Human Embryonic Kidney (HEK293T) cell line is a highly transfectable version of SV40 T-antigen containing 293 human embryonic kidney cells. The FreeStyle 293-F cell line is a version of 293 cells that are adapted to suspension culture in FreeStyle 293 Expression Medium. TZM-bl is a HeLa reporter cell line expresses CD4 receptor and CXCR4 and CCR5 chemokine co-receptors and luciferase and b-galactosidase genes under the control of the HIV-1 promoter, hence is useful to assay in-vitro HIV infection.

METHOD DETAILS

SIV Envelope Trimer Design, Expression, and Purification

SOSIP.664 HIV Env trimer modification were incorporated into envelope encoding sequences corresponding to four Chimpanzee (SIVcpz*Ptt*) isolates (GAB1 [GenBank: P17281]; MB897 [GenBank: ABU53023]; EK505 [GenBank: ABD19499]; and MT145 [GenBank: ABD19508]) to express as soluble native-like trimers as described previously (Sanders et al., 2013). Briefly, the following modifications were incorporated into these Envs for soluble trimer expression: a) the Env leader sequence was replaced by Tissue Plasminogen Activator (TPA) signal sequence for higher protein expression; b) a disulfide bond was introduced between gp120 and gp41 subunits by substituting residues A501-C and T605-C respectively in gp120 and gp41; c) the gp120 REKR cleavage site was replaced by Furin inducible R6 site (RRRRRR) for enhancing cleavage efficiency between gp120 and gp41; and d) an I559P substitution in gp41 to stabilize the soluble trimer protein. In addition, a GS-linker and a His-tag were added to the $gp41_{ECTO}$ C terminus at HXB2 residue 664 position. The codon-optimized SOSIP.664 gp140 gene constructs were synthesized (Geneart, Life Technologies) and cloned into the phCMV3 vector (Genlantis). Recombinant envelope proteins were expressed in HEK293F cells as described elsewhere (Sanders et al., 2013). Briefly, HIV Env trimers CRF250, WITO, C108, ZM197-ZM233V1V2 and the 4 chimpanzee SIV SOSIP.664 Env-encoding trimer plasmids were cotransfected with a plasmid encoding for Furin (3:1 ratio) into HEK293F cells using

PEI-MAX 4000 transfection reagent (*Polysciences, Inc.*). The secreted soluble trimers proteins were purified from cell supernatants after 5 days using agarose-bound Gallanthus Nivalis Lectin (GNL) (Vector Labs) or CNBr-activated Sepharose 4B bead (GE Healthcare) bound PGT145 bnAb antibody affinity columns as described previously (Pugach et al., 2015). The affinity-purified proteins were size exclusion chromatography (SEC)-purified with a Superdex 200 10/300 GL column (GE Healthcare) in PBS/TBS. The purified trimers for the immunization experiments were quality control tested for antigenicity with a range of HIV Env-specific neutralizing and non-neutralizing mAbs.

Antibodies, Expression, and Purification

HIV envelope specific mAbs to a broad range of epitopes were used, including those that target V2-apex, V3-N332, linear V3, CD4bs, CD4i and gp120-41 Env sites. A dengue antibody (DEN3) was used as control Ab for binding experiments. For PG9 and CH01 V2-apex bnAb inferred germline antibody designs, the heavy and the light chain V-gene of the mature Abs were reverted to their corresponding closest inferred germline gene sequence as determined using the ImMunoGeneTics (IMGT) website (http://imgt.cines.fr/) (Brochet et al., 2008). The reverted variable heavy and light chain nucleotide sequences were synthesized by Geneart (Life Technologies) and cloned into corresponding Igγ1, Igκ, and Igλ expression vectors as previously described (Tiller et al., 2008), using the Gibson cloning method (NEB, USA). The antibodies were expressed and purified using methods described previously (Sok et al., 2014b). Briefly, the heavy and light chain encoding plasmids were reconstituted (1:1 ratio) in Opti-MEM (Life Technologies), and cotransfected HEK293F cells (Invitrogen) using 293fectin (Invitrogen). The suspension cells were cultured for 4-5 days in a shaker incubator at 8% CO2, 37.0°C, and 125 rpm. The antibody containing supernatants were harvested, filtered through a 0.22 mm Steriflip units (EMD Millipore) and passed over a protein A or protein G affinity column (GE Healthcare). The bound antibody was eluted from the columns in 0.1 M citric acid, pH 3.0. Column fractions containing IgG were neutralized (2M Tris-base), pooled, and dialyzed against phosphate-buffered saline (PBS), pH 7.4. IgG purity was determined by sodium dodecyl sulfate-polyacrylamide gel electrophoresis, and the concentration was determined by measuring the relative absorbance at 280 nm.

Site-Directed Mutagenesis

The amino-acid point mutations in Env-encoding plasmids were incorporated by using a QuikChange site-directed mutagenesis kit (Agilent Technologies, USA), according to the manufacturer's instructions. All of the mutations were confirmed by DNA sequence analysis (Eton Bioscience, San Diego, CA).

Differential Scanning Calorimetry

Thermal denaturation was analyzed with a differential scanning calorimetry (DSC) using a MicroCal VP-Capillary DSC instrument (Malvern), at a scanning rate of 1 K/min under 3.0 atmospheres of pressure. Samples were dialyzed in PBS pH 7.4 overnight and protein concentration was adjusted to 0.5 mg/mL prior to measurement. DSC data were analyzed after buffer correction, normalization, and baseline subtraction using MicroCal VP-Capillary DSC analysis software provided by the manufacturer.

Negative Stain Electron Microscopy and Data Treatment

Purified M145K sample was deposited on thin-carbon-coated (Edward Auto 306 carbon evaporator) a C-flat EM grid (Cu400 mesh, 2 μm hole diameter, 2 μm hole spacing) (Protochips, Morrisville, NC, USA) and embedded in 2% (w/V) uranyl formate. The carbon-coated grids were Ar/O_2-plasma-cleaned (Gatan Solarus Model 950 Advanced Plasma System; Gatan Inc., Pleasanton, CA, USA) prior to sample deposition. The uranyl-stained EM sample was then inserted into an FEI Tecnai 12 microscope (Thermo Fisher Scientific, Waltham, MA, USA) equipped with a US4000 CMOS detector (Gatan Inc., Pleasanton, CA, USA). The data was collected at 52,000X nominal magnification resulting in a pixel size of 2.05Å at the object level. Data was binned by a factor of 2 prior to data treatment. Projection image identification in the micrographs was performed with a difference-of-Gaussians implementation (Voss et al., 2009). Projection images subsequently underwent 2D alignment and classification by iterative multi-reference alignment/multivariate statistical analysis (Ogura et al., 2003).

CryoEM Sample Preparation, Data Collection, Processing, and Analysis

Purified MT145K sample was deposited on a C-flat EM grid (Cu400 mesh, 2 μm hole diameter, 2 μm hole spacing) (Protochips, Morrisville, NC, USA) that had been Ar/O_2-plasma-cleaned (Gatan Solarus Model 950 Advanced Plasma System; Gatan Inc., Pleasanton, CA, USA) prior to sample deposition. Excess buffer was then blotted away from the grid followed by plunging into and vitrification in liquid ethane cooled by liquid nitrogen using a vitrobot (Thermo Fisher Scientific, Waltham, MA, USA). The resulting cryo-EM specimen was transferred into an FEI Titan Krios microscope (Thermo Fisher Scientific, Waltham, MA, USA) equipped with a Gatan K2 Summit direct electron detector (Gatan Inc., Pleasanton, CA, USA). Dose-fractionated data was collected in electron counting mode at a nominal magnification of 29,000X resulting in a pixel size of 1.02 Å at the object level. Micrograph movie frame exposure time was 200ms and each movie micrograph was recorded over 10 s (50 movie frames) corresponding to a total dose of 94e^-/Å^2. Movie micrograph frames were subsequently aligned (MotionCor2; (Zheng et al., 2017)), dose-weighted and signal-integrated resulting in 1,281 micrographs for further data processing. CTF models were determined using GCTF (Zhang, 2016). Candidate projection images of MT145K were identified using a difference-of-Gaussians implementation (Voss et al., 2009). The resulting set of candidate projection images subsequently underwent 2D alignment and classification by use of Relion 2.1b1 (Scheres, 2012).

~95,000 projection images corresponding to well-formed class averages of MT145K were selected for further data processing. This data class was iteratively angularly refined and reconstructed using a B41 unliganded Env trimer map rendered at 60 Å resolution as an initial reference (Ozorowski et al., 2017). The data class then underwent 3D classification into six classes with the initial reconstruction rendered at 60 Å resolution as reference. From 3D classification, a subset of 44,301 projection images was selected for final data processing comprising CTF model adjustment at the projection-image level (Zhang, 2016) and angular refinement and reconstruction (Scheres, 2012).

Model Building and Refinement

A homology model (Modeler; (Webb and Sali, 2016)) was generated from sequence alignment of MT145K and BG505 and the structure of the latter (PDB: 4TVP). Significant manual rebuilding followed in Coot (Emsley and Cowtan, 2004). A fragment library was then created from the MT145K sequence containing 200 homologous, non-redundant sequences at each MT145K 7-mer position. Library fragment-based, density-guided, real-space rebuilding was then performed (DiMaio et al., 2015) with 319 decoys. The resulting models were evaluated geometrically (MolProbity; (Chen et al., 2010)) and by fit-to-map (EMRinger; (Barad et al., 2015). The overall best model was selected for further iterations of manual rebuilding and multi-decoy, density-guided, real-space, all-atom Rosetta FastRelax refinement. Finally, glycans were manually built in Coot and restricted, density-guided real-space refinement performed in Phenix 1.12 (Adams et al., 2002) followed by model evaluation by MolProbity, EMRinger and Privateer (Agirre et al., 2015).

Global N-Linked Glycan Analysis

The quantifications and structural characterization of the total glycan pool was achieved by cleaving the N-inked glycans from the surface of the glycoprotein using an in-gel digestion with peptide N-glycosidase F (PNGaseF). The resultant glycans were separated into two aliquots. The first was derivatized with 2-aminobenzoic acid (2-AA) and subjected to HILIC-UPLC analysis using an Acquity UPLC (Waters). To quantify the oligomannose content of the released glycans, the labeled samples were treated with endoglycosidase H (endoH), which selectively cleaves oligomannose glycans. Data analysis and interpretation were performed using Empower software (Waters). The second aliquot of released glycans was subjected to negative ion electrospray ion mobility mass spectrometry using a Synapt G2Si mass spectrometer (Waters). Glycan compositions were determined using collision induced dissociation (CID) fragmentation. Data analysis was performed using Waters Driftscope (version 2.8) software and MassLynxTM (version 4.1). Spectra were interpreted as described previously (Harvey et al., 2009). The glycan compositions were used to generate a sample-specific glycan library that was used to search the glycopeptide data to minimize the number of false-positive assignments in site-specific analysis.

LC-MS Glycopeptide Analysis

Site-specific N-glycosylation analysis was performed using proteolytic digestion followed by tandem LC-MS. Prior to digestion, trimers were denatured, reduced and alkylated by incubation for 1h at room temperature (RT) in a 50 mM Tris/HCl, pH 8.0 buffer containing 6 M urea and 5 mM dithiothreitol (DTT), followed by the addition of 20 mM iodacetamide (IAA) for a further 1h at RT in the dark, and then additional DTT (20 mM) for another 1h, to eliminate any residual IAA. The alkylated trimers were buffer-exchanged into 50 mM Tris/HCl, pH 8.0 using Vivaspin columns (GE healthcare) and digested separately with trypsin, elastase and chymotrypsin (Mass Spectrometry Grade, Promega) at a ratio of 1:30 (w/w). Glycopeptides were selected from the protease-digested samples using the ProteoExtract Glycopeptide Enrichment Kit (Merck Millipore) following the manufacturer's protocol. Enriched glycopeptides were analyzed by LC-ESI MS on an Orbitrap fusion mass spectrometer (Thermo Fisher Scientific), as previously described (Behrens et al., 2016), using higher energy collisional dissociation (HCD) fragmentation. Data analysis and glycopeptide identification were performed using ByonicTM (Version 2.7) and ByologicTM software (Version 2.3; Protein Metrics Inc.), as previously described (Behrens et al., 2016).

Glycan Modeling

$Man_9GlcNAc_2$ oligomannose-type glycans were docked and rigid-body fitted at each of the corresponding Env glycan positions using the MT145K structure presented here or an unliganded BG505 SOSIP.664 structure (PDB: 4ZMJ).

Pseudovirus Production

To produce pseudoviruses, Env-encoding plasmids were cotransfected with an Env-deficient backbone plasmid (pSG3ΔEnv) (1:2 ratio) using X-tremeGENE 9 (Sigma-Aldrich) DNA transfection reagent. Briefly, $1X10^6$ cells in 10ml of Dulbecco's Modified Eagle Medium (DMEM) were seeded in a 100mm x 20mm cell culture dish (Corning) one day prior to transfection. For transfection, 40μl of X-tremeGENE 9 was added to 700μl of Opti-MEM I reduced serum medium (Thermo Fisher) in tube 1. The Env-encoding plasmid (5 μg) and pSG3ΔEnv (10 μg) were added to tube 2 in 700μl of Opti-MEM. The tube 1 and tube 2 solutions were mixed together and incubated for 25 min at room temperature. Next, the transfection mixture was added to the media with 293T cells seeded previously and then distributed uniformly. All pseudoviruses were harvested 48-72 h posttransfection, filtered through 0.22 mm Steriflip units (EMD Millipore) and aliquoted for use in neutralization assays.

Neutralization Assay

Neutralization was measured by using single-round replication-defective HIV Env-pseudoviruses and TZM-bl target cells (Montefiori, 2005; Seaman et al., 2010). 25ul of 3-fold serially diluted mAbs or serum samples were pre-incubated at 37°C for 1h with 25ul of tissue culture infective dose-50 (TCID50) Env-pseudotyped virus in a half-area 96-well tissue culture plate. TZM-bl target cells (5,000 cells/well) in 50μl of DMEM were added and the plates were allowed to grow in humidified incubator at 37°C and 5% Co_2. The luciferase activity of the lysed cells was read on instrument (Biotek) after 2-3 days, by adding lysis buffer followed by Brightglow (Promega). The 50% inhibitory concentration (IC_{50}) or 50% inhibitory doses (ID_{50}) was reported as the antibody concentration or serum dilution required to reduce infection by half.

ELISA Binding Assay

ELISA binding experiments were performed as described previously with minor modification (Sanders et al., 2013). ELISA binding with SOSIP.664 trimer proteins with mAbs was carried out by either capturing the trimer proteins onto the anti-His capture antibodies or on the streptavidin coated plates through biotinylated trimers. For trimer biotinylation, the SOSIP.664 proteins were randomly biotinylated using a 2:1 molar ratio of biotin reagent to trimer using the EZ-link-NHS-PEG4-Biotin kit (Thermo Fisher Scientific, 21324). MaxiSorp plates (Thermo Fisher Scientific) were coated overnight at 4C with 2 ug/mL of anti-His Ab (Thermo Fisher Scientific) or 2 ug/mL streptavidin (Thermo Fisher Scientific). Plates were blocked for 1 hr with 3% BSA and washed three times with 0.05% Tween 20-PBS (PBS-T) (pH 7.4). Anti-His or Streptavidin-coated plates were incubated with biotinylated trimers in 1%BSA plus PBST for 1.5 hr and washed three times with PBST. 3-fold serially diluted mAbs or sera were added starting at a maximum concentration of 10 ug/mL (100ug/ml for iGL Abs) (sera at 1:100 dilution) in 1% BSA plus PBST, and incubated at room temperature (RT) for 1.5 hr. Plates were washed three times with PBST. Alkaline-phosphatase-conjugated goat anti-human IgG Fc secondary antibody (Jackson ImmunoResearch Laboratories) was diluted 1:1000 in 1% BSA PBST and added to plates for 1 hr at RT. Plates were washed three times with PBST and incubated with phosphatase substrate (Sigma) for 15 mins and the absorbance at 405 nm recorded. The 50% binding (EC_{50}) was recorded as the half of the maximum binding activity and was calculated by linear regression method using Prism 6 Software.

Bio-Layer Interferometry (BLI) Binding Assay

The binding experiments of Abs to the affinity purified trimers were performed with an Octet K2 system (ForteBio, Pall Life Sciences). Briefly, the mAbs or IgGs (10 ug/mL in PBST) were immobilizing onto hydrated anti-human IgG-Fc biosensors (AHC: ForteBio) for 60 s to achieve a binding response of at least 1.0. After Ab capture, the sensor was placed in a PBST wash buffer to remove the unbound Ab to establish a baseline signal. Next, the IgG immobilized sensor was dipped into a solution containing SOSIP.664 trimer protein as analyte and incubated for 120 s at 1000 rpm. Following this, the trimer bound to IgG immobilized sensor was removed from the analyte solution and placed into the PBST buffer for 240 s at 1000 rpm. The 2- and 4-minute binding intervals respectively denote the association and dissociation binding curves reported in this study. The sensograms were corrected with the blank reference and fit (1:1 binding kinetics model) with the ForteBio Data Analysis version.9 software using the global fitting function. The data are represented as maximum binding response or the association and dissociation curve fits.

Trimer Protein Immunizations in CH01 UCA HC-Only KI Mice

For the immunization experiments, groups of 5 CH01 UCA HC-only knock-in B cell expressing mice were immunized with 25ug of the individual trimer protein or 25ug total protein of the 3-trimer cocktail (Prime, week-0; Boost-1, week-4 and Boost-2, week-8) along with Glucopyranosyl Lipid Adjuvant in stable emulsion (GLA-SE) as adjuvant. Immunizations were administered intramuscular in the leg of each animal with 25 μg of total trimer immunogens. Blood samples were collected at pre-bleed (Pre), and 2-weeks post-prime (Bleed #1), 2-weeks post boost-1 (Bleed #2), 4-weeks post boost-1 prior to HIV trimer boosting (Bleed #3), and post boost-2 (Bleed #4) immunization time-points for the isolation of sera that were tested for presence of neutralizing antibodies in TZM-bl cell based assay. Serum samples were heat inactivated for potential complement activity at 56°C for 0.5 h. Mice used in this study were approved by Duke University Institutional Animal Care and Use Committee-approved animal protocols.

QUANTIFICATION AND STATISTICAL ANALYSIS

Statistical Analysis

Statistical analysis was performed using Graph Pad Prism 7 for Mac, Graph Pad Software, San Diego, California, USA. The IC_{50} virus neutralization and the EC_{50} trimer binding Ab titers with MT145K were compared by two-tailed nonparametric Spearman correlation test with 95% Confidence interval. P value of less than 0.05 were treated as significant. Cryo-EM data were analyzed by a difference-of-Gaussian approach (DoG-Picker) to identify molecular projection images for further processing. Maximum Likelihood optimization (RELION) was utilized to determine a subset of data (44,301 molecular projection images) most suitable for refinement to highest possible resolution and to determine projection image Euler angles and planar shifts.

DATA AND SOFTWARE AVAILABILITY

Cryo-EM reconstructions have been deposited in the Electron Microscopy Data Bank (EMDB) under the accession numbers EMD-20074 and the PDB code for this deposition is 6OHY. The GenBank accession numbers for the heavy and light chain inferred germline versions of PG9 and CH01 broadly neutralizing antibodies reported in this paper are MK825341-MK825344.

Cell Reports, Volume *27*

Supplemental Information

The Chimpanzee SIV Envelope Trimer:

Structure and Deployment as an HIV Vaccine Template

Raiees Andrabi, Jesper Pallesen, Joel D. Allen, Ge Song, Jinsong Zhang, Natalia de Val, Gavin Gegg, Katelyn Porter, Ching-Yao Su, Matthias Pauthner, Amanda Newman, Hilary Bouton-Verville, Fernando Garces, Ian A. Wilson, Max Crispin, Beatrice H. Hahn, Barton F. Haynes, Laurent Verkoczy, Andrew B. Ward, and Dennis R. Burton

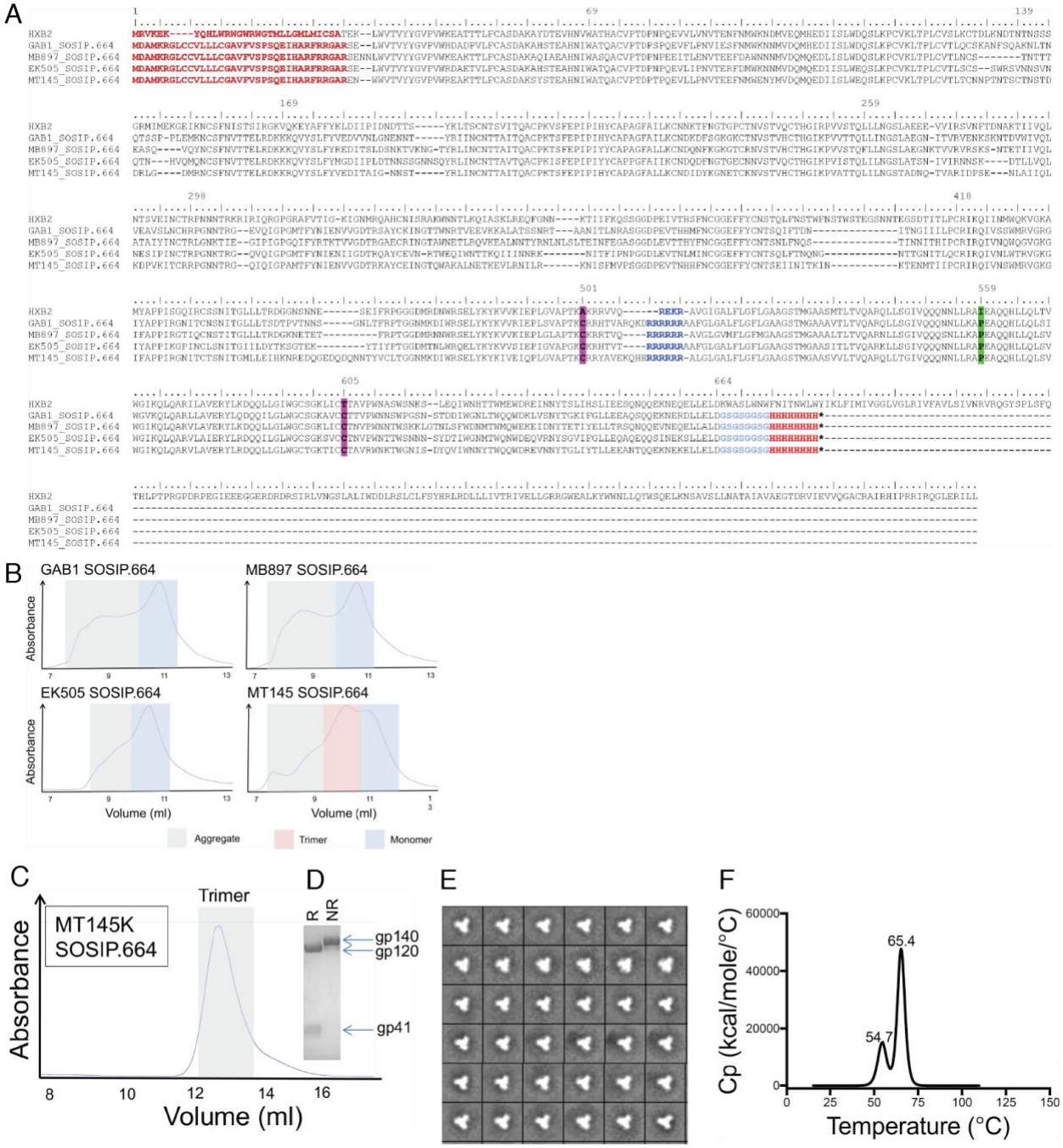

Figure S1. Design and purification of SIVcpz*Ptt* envelope derived SOSIP.664 trimers and characterization of MT145K trimer. Related to Figures 1 and 2.

A. Amino-acid sequence alignment of 4 SIVcpz*Ptt* envelope sequences (GAB1, MB897, EK505 and MT145) with reference HIV Env sequence, HXB2, showing SOSIP.664 trimer stabilizing modifications. The soluble SOSIP.664 trimer modifications include: (i) incorporation of a disulfide bond between residue 501 of gp120 (A501C) and residue 605 of gp41 (T605C), (ii) replacing naturally occurring gp120 and gp41 cleavage site with R6-cleavage site (shown in blue), (iii) I559P substitution in the gp41, (iv) and a truncation in the gp41 subunit at residue 664.

B. Size Exclusion Chromatography (SEC) profiles of *Gallanthus nivalis* lectin (GNL) purified trimers on Superdex 200 Increase 10/300 GL column. The SEC profiles show the aggregate/trimer-dimer, trimer and monomer peaks of the GNL-purified proteins. The MT145 SOSIP.664 trimer showed substantial protein fractions that assemble as a trimer.

C. Size exclusion chromatography (SEC) of PGT145 antibody purified MT145K SOSIP.664 trimer reveals trimer eluting as a single peak with no aggregation.
D. SDS-PAGE of MT145K trimer protein under non-reducing (NR) and reducing (R) conditions (reducing agent DTT was added). The MT145K trimer is efficiently cleaved into gp120 and gp41 subunits.
E. Negative Stain Electron-Microscopy (NS-EM) of MT145K trimer: 2D class averages show that trimers adopt well-ordered, native-like conformations.
F. Thermostablity of the MT145K trimer. Thermal denaturation of the MT145K trimer by Differential Scanning Calorimetry (DSC) reveals a major trimer population melting at a T*m* of 65.4 °C.

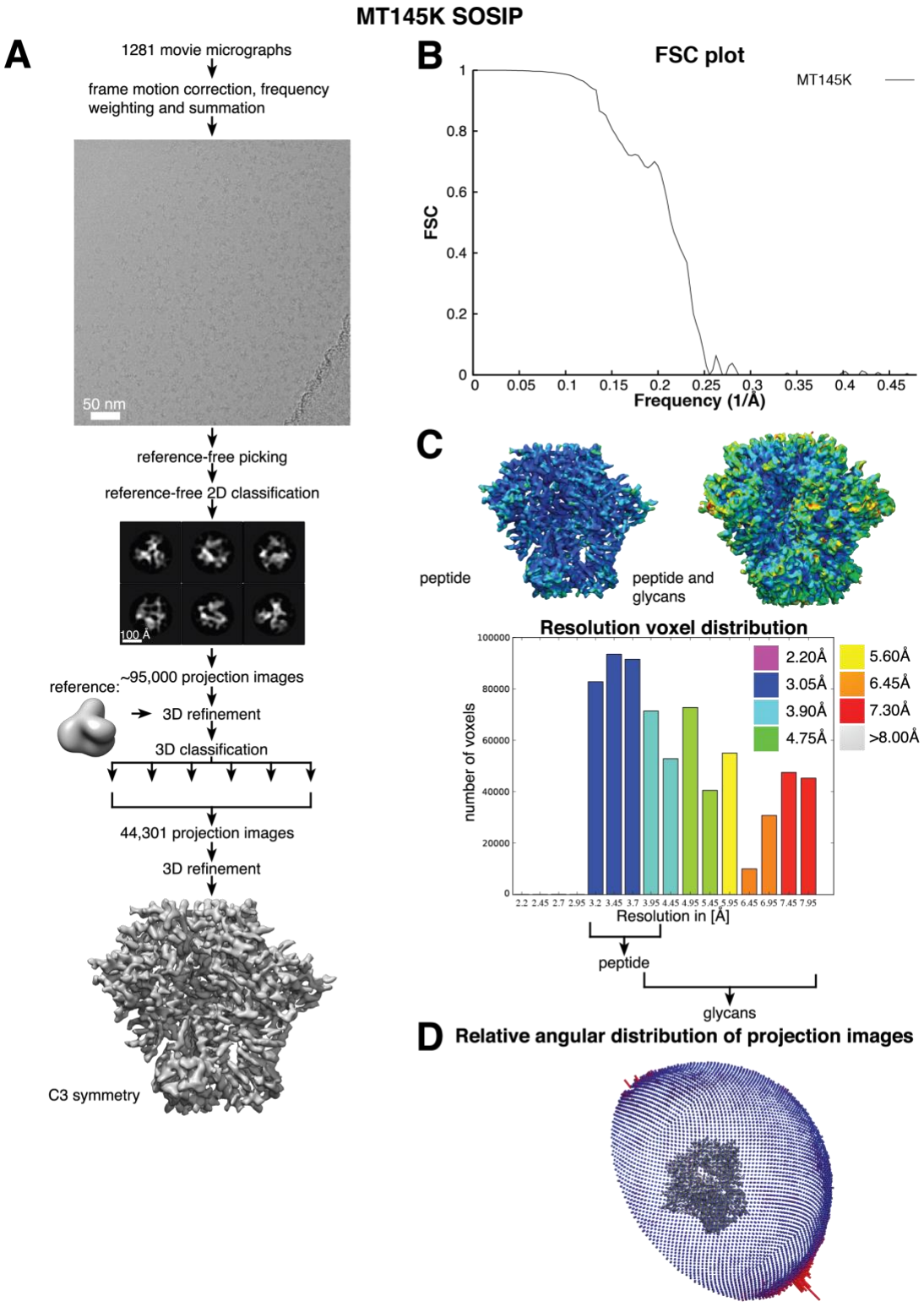

Figure S2. Structural analysis of MT145K by cryo-electron microscopy. Related to Figure 2.
A. Cryo-EM data processing flow diagram resulting in a density map at ~4.1Å global resolution.
B. FSC between two independently refined data half sets.
C. Local resolution in the MT145K density map. The peptide part of MT145K is resolved primarily in the 3.0-4.0 Å range, whereas the glycan shield overall is resolved to significantly lower resolutions.
D. Angular distribution of the angularly refined data class giving rise to the final reconstruction.

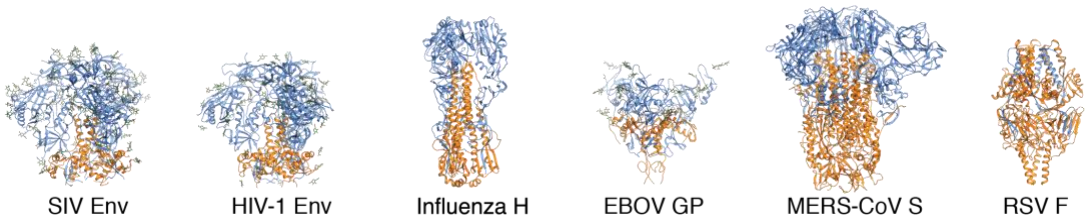

Figure S3. Comparison of Env trimer architectures of class I fusion proteins. Related to Figure 2.
Prefusion SIV Env (MT145K; current study) follows an overall organization similar to other known prefusion class I fusion proteins. Fusion subunits (shown in orange) are most commonly organized membrane-proximally (RSV F deviating somewhat from this trend). Fusion subunits are largely shielded and capped by receptor-recognizing subunits (shown in cornflower blue) in the meta-stable prefusion state. SIV Env is most similar to HIV Env; however, MT145K is less compact than the displayed HIV Env trimer (BG505 isolate). The more open organization of MT145K may be the result of its fusion peptide being inserted into a pocket at the gp120/gp41 interface as opposed to the fusion peptide found on the outside of the HIV Env trimer (MT145K: current study, HIV: PDB 4ZMJ (Kwon et al., 2015); Influenza A H1N1: PDB 1RD8 (Stevens et al., 2004); Ebola virus GP: PDB 5KEL (Pallesen et al., 2016); MERS-CoV S: PDB 5W9J (Pallesen et al., 2017); RSV F: PDB 4JHW (McLellan et al., 2013).

A

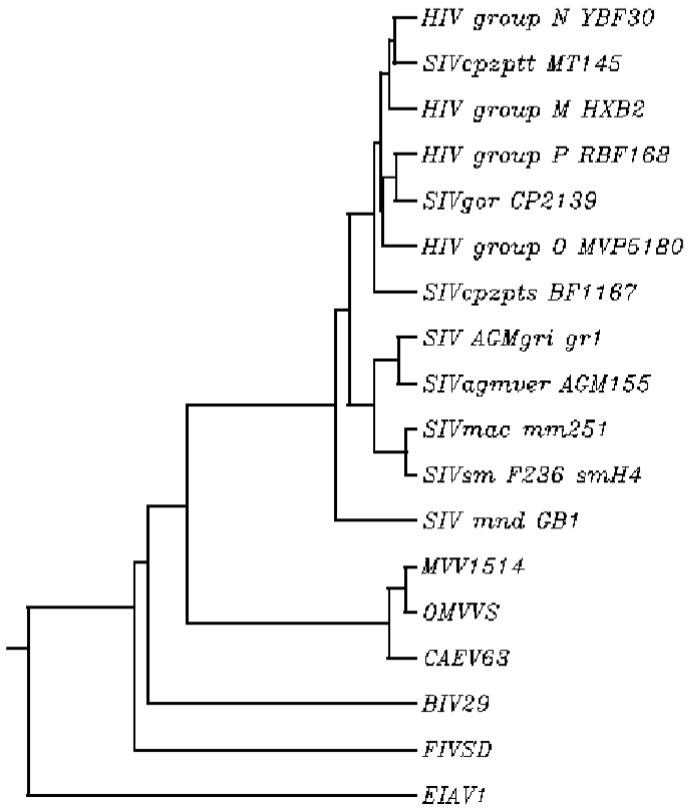

B

Env length (AA)	PNGS	Glycan density
842	29	3.44
855	27	3.16
856	31	3.62
882	30	3.40
872	30	3.44
876	32	3.65
884	26	2.94
854	24	2.81
768	22	2.86
881	24	2.72
885	24	2.71
821	20	2.44
982	29	2.95
990	28	2.83
942	28	2.97
904	19	2.10
854	22	2.58
859	19	2.21

Figure S4. Phylogeny of lentiviruses and the glycan shield density. **Related to Figure 3.**

A. Phylogenetic relationships among the envelope sequences derived from various lentiviruses; tree constructed by maximum likelihood method. These lentiviruses infect host species that include equine (EIAV), feline (FIV), bovine (BIV), caprine/ovine (CAEV, OMVVS and MVV), simian (SIV) and humans (HIV).

B. The number of amino acids and the number of Potential N-linked Glycan Sites (PNGS: predicted by N-GlycoSite tool at Los Alamos HIV database) in the full-length envelopes are listed for each lentivirus. The glycan shield density for each virus is represented as % Env residues that encode PNGS motifs and was calculated by (number of PNGS / Env length x 100). The glycan shield density shows a gradual increase from EIAV through CAEV, and plateaus in some of the SIV species including SIVcpz*Ptt*, the one that has been shown to have crossed into humans.

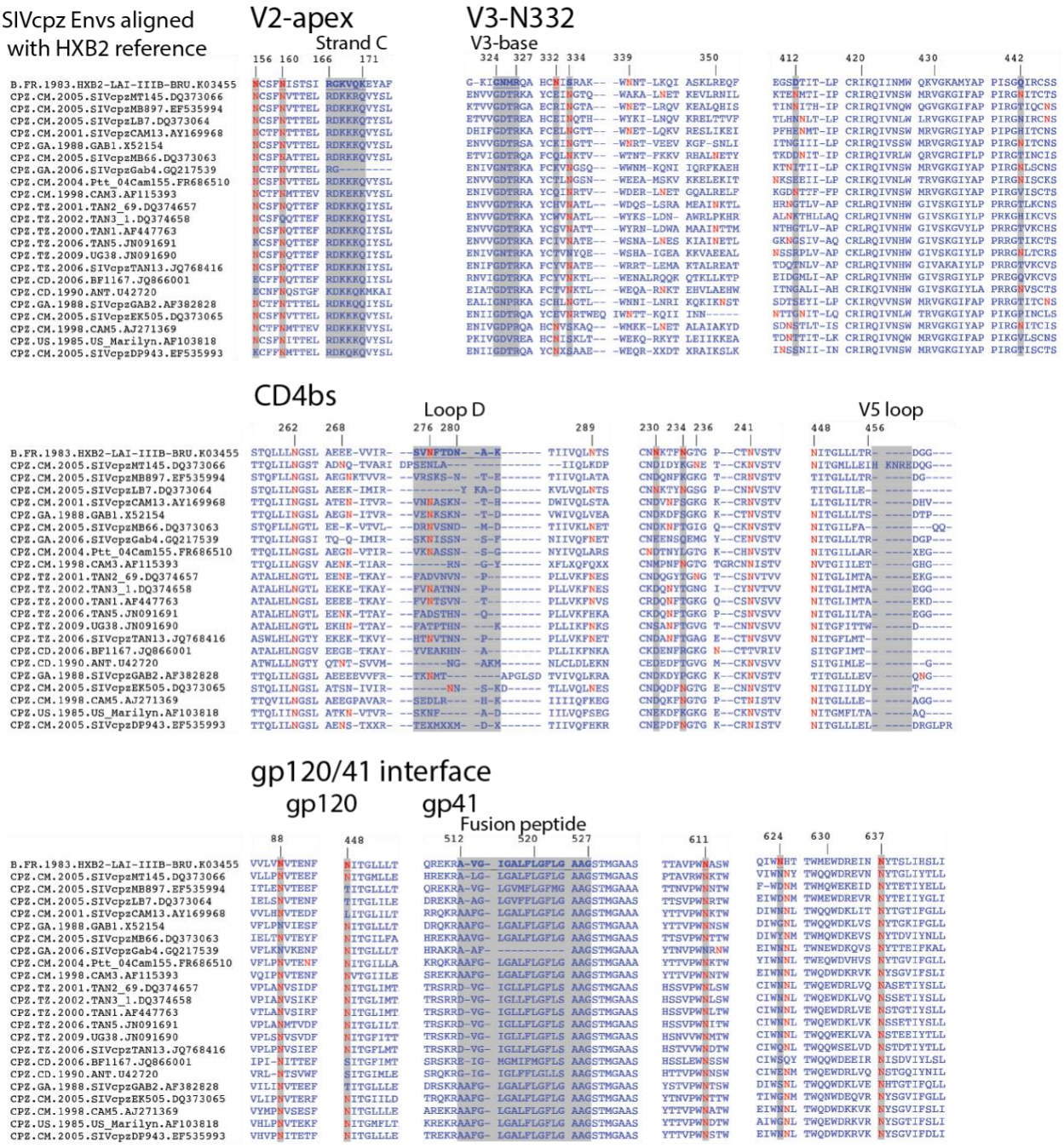

Figure S5. Amino-acid sequence alignment of SIV envelopes with HXB2 HIV Env as a reference depicting SIV Env residues equivalent to HIV bnAb epitopes. Related to Figures 3, 4 and 5.

The amino-acid alignment of SIVcpz*Ptt* envelope sequences compared to the HXB2 reference sequence. The protein residues (highlighted in grey) and the N-glycosylation sites (depicted in red) for each bnAb epitope region (V2-apex, V3-N332, CD4bs and gp120-gp41 interface) are shown.

Epitope	Antibody	MT145K Virus IC50	MT145K Trimer EC50	MT145K gp120 EC50	BG505 Trimer IC50
V2 Apex	PG9	0.008	0.055	0.792	0.03
	PG16	0.005	0.054	>10	0.01
	CH01	0.173	0.187	>10	0.53
	CH02	0.271	0.487	>10	0.46
	CH03	0.165	0.714	>10	>10
	CH04	0.256	0.453	>10	0.50
	PGT141	5.558	0.083	>10	0.04
	PGT142	5.779	0.075	>10	0.05
	PGT143	5.837	0.046	>10	0.04
	PGT144	>10	>10	>10	1.78
	PGT145	0.151	0.029	>10	0.02
	PGDM1400	0.010	0.018	>10	<0.003
	CAP256.01	0.121	0.130	>10	>10
	CAP256.02	0.013	0.049	>10	>10
	CAP256.03	<0.003	0.044	>10	3.25
	CAP256.04	0.004	0.076	>10	5.49
	CAP256.05	0.004	0.036	>10	>10
	CAP256.06	1.624	0.070	>10	>10
	CAP256.07	0.023	0.099	>10	>10
	CAP256.08	<0.003	0.037	>10	0.01
	CAP256.09	<0.003	0.041	>10	0.07
	CAP256.10	0.016	0.062	>10	>10
	CAP256.11	0.026	0.053	>10	>10
	CAP256.12	0.440	0.090	>10	>10
	CAP256.I1	3.713	0.122	>10	>10
	CAP256.I2	0.026	0.056	>10	>10
	2909	>10	>10	>10	>10
	C108G	>10	>10	>10	>10
	830A	>10	>10	>10	>10
	697	>10	>10	>10	>10

Epitope	Antibody	MT145K Virus IC50	MT145K Trimer EC50	MT145K gp120 EC50	BG505 Trimer IC50
V3-N332	PGT121	>10	>10	>10	0.03
	PGT122	>10	>10	>10	0.05
	PGT123	>10	>10	>10	4.74
	PGT124	>10	>10	>10	>10
	PGT125	>10	>10	>10	0.09
	PGT126	>10	>10	>10	0.45
	PGT127	>10	>10	>10	0.09
	PGT128	>10	>10	>10	0.05
	PGT130	>10	>10	>10	0.09
	PGT131	>10	>10	>10	>10
	PGT133	>10	>10	>10	0.01
	10-1074	>10	>10	>10	0.03
	PGT135	>10	>10	>10	>10
	PGT136	>10	>10	>10	>10
	PGT137	>10	>10	>10	>10
	2G12	>10	>10	>10	>10
V3	447-52D	>10	>10	>10	>10
	2557	>10	>10	0.483	>10
	4022	>10	>10	>10	>10
	3074	>10	>10	0.451	>10
	3791	>10	>10	>10	>10
	3904	>10	>10	0.242	>10
	4508	>10	>10	>10	>10
	537	>10	>10	>10	>10
	15e	>10	>10	>10	>10
	19b	ND	>10	>10	>10
	14e	ND	>10	0.138	>10

Epitope	Antibody	MT145K Virus IC50	MT145K Trimer EC50	MT145K gp120 EC50	BG505 Trimer IC50
CD4bs	VRC01	>10	>10	>10	0.07
	VRC03	>10	>10	>10	1.82
	VRC06	>10	>10	>10	>10
	HJ16	>10	>10	>10	>10
	12A12	>10	>10	>10	0.04
	NIH45-46	>10	>10	>10	0.02
	PGV04	>10	>10	>10	0.05
	CH103	>10	>10	>10	3.72
	3BNC60	>10	>10	>10	0.01
	3BNC117	>10	>10	>10	0.01
CD4bs	b6	>10	>10	>10	>10
	b12	>10	>10	>10	>10
	F105	>10	>10	>10	>10
CD4i	A32	>10	>10	>10	>10
	17b	>10	8.834	5.8	>10
	E51	>10	>10	>10	>10
CD4bs	CD4-IgG2	0.456	0.562	6.500	ND

Epitope	Antibody	MT145K Virus IC50	MT145K Trimer EC50	MT145K gp120 EC50	BG505 Trimer IC50
Gp120-41	PGT151	>10	1.427	>10	<0.003
	PGT152	>10	>10	>10	<0.003
	PGT153	>10	>10	>10	0.028
	PGT154	>10	>10	>10	<0.003
	PGT155	>10	>10	>10	<0.003
	PGT156	>10	>10	>10	<0.003
	PGT157	>10	>10	>10	<0.003
	PGT158	>10	>10	>10	<0.003
	8ANC195	>10	>10	>10	0.091
	35022	<0.003	0.337	>10	>10
Gp41	F240	>10	>10	>10	>10
Dengue	DEN3	>10	>10	>10	>10

IC50/EC50	Color Scale
>10	
10	
1	
0.1	
0.01	
0.003	
<0.003	
ND	Not determined

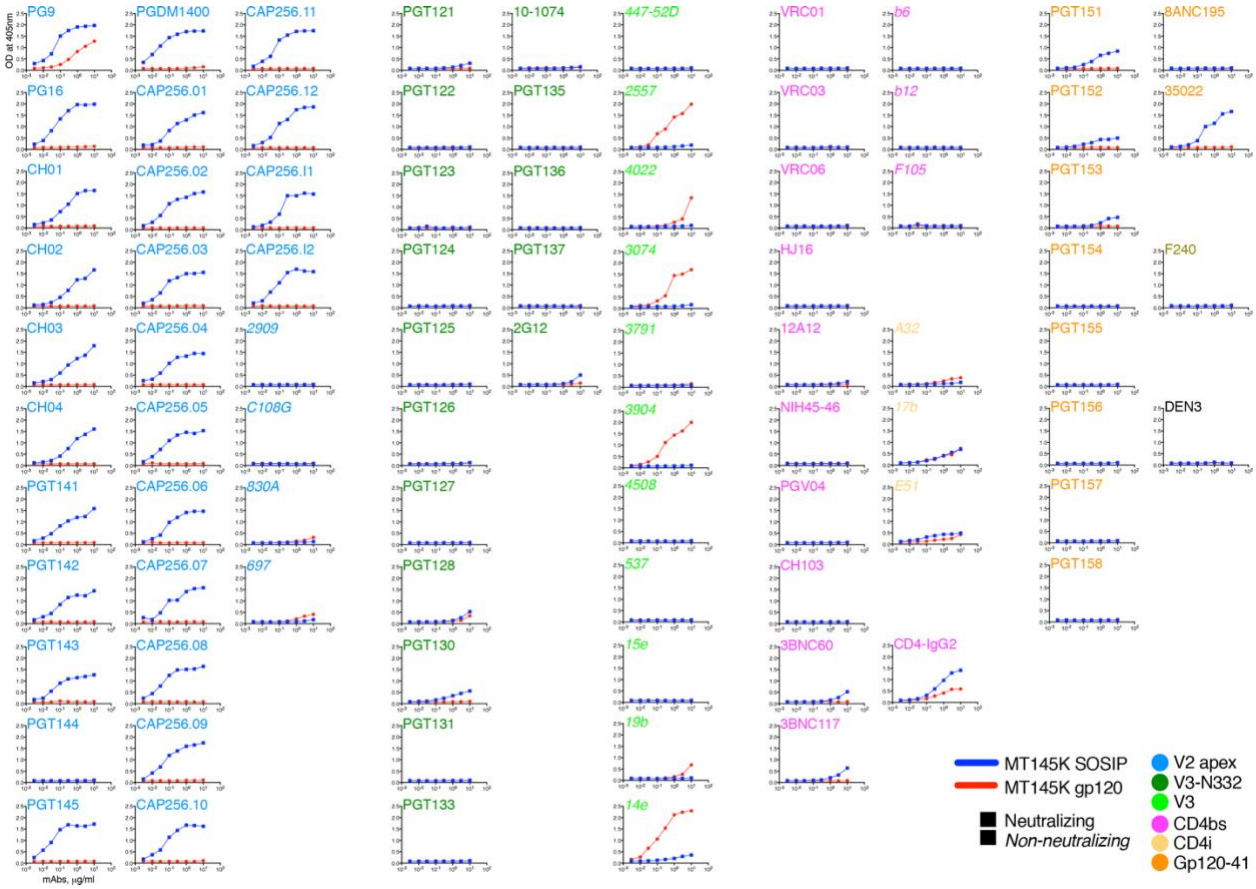

Figure S6. Antigenic profile of various MT145K Env forms with HIV Env-specific mAbs. Related to Figure 4. Neutralizing and non-neutralizing HIV Env-specific mAbs targeting various epitope specificities, including V2-apex, V3-N332, linear V3, CD4bs, CD4i and gp120-gp41 interface were tested with MT145K and BG505 Env-encoding pseudoviruses in a neutralization assay and against the MT145K SOSIP trimer and MT145K gp120 monomer by ELISA. The reciprocal IC_{50} neutralization titers against the MT145K and BG505 viruses and the 50% ELISA binding titers (EC_{50} binding with trimer and gp120 proteins) for each mAb are shown. ELISA binding curves of the HIV Env specific mAbs to the soluble MT145K trimer (blue) and its monomeric gp120 (red) protein. HIV Env mAbs specificities are shown in different colors. V2-apex directed mAbs display a strong binding with the MT145K trimer. Binding curves also reveal weak but detectable binding activities of the mAbs recognizing various HIV Env specificities (PGT121, PGT128, PGT130, 2G12, 14e, 3BNC60, 3BNC117, E51, PGT152 and PGT153).

Figure S7. BioLayer Interferometry (BLI) binding responses of the HIV Env specific mAbs to the soluble MT145K trimer and MT145K monomeric gp120 proteins. Related to Figure 4.

BLI or octet binding curves (association: 120s; (0-120) and dissociation: 240s; (120-360)) of the HIV Env specific mAbs with soluble MT145K trimer (blue) and its monomeric gp120 (red) protein. 10µg/ml final concentration of the HIV mAbs recognizing a range of Env epitope specificities (mAbs names shown in different colors indicate the corresponding specificity) were captured onto an anti-human IgG-Fc sensor (AHC: ForteBio.) to achieve at least 1 RU binding response. The immobilized IgG biosensors were immersed in the 200nM MT145K trimer or 500nM MT145K gp120 solution as the analyte and the binding curves are shown as association and dissociation of Ab-protein interactions. In addition to the V2-apex directed mAbs, a few of the V3-N332 glycan mAbs, PGT121, PGT125, PGT130 and 2G12 exhibited weak binding with the MT145K trimer.

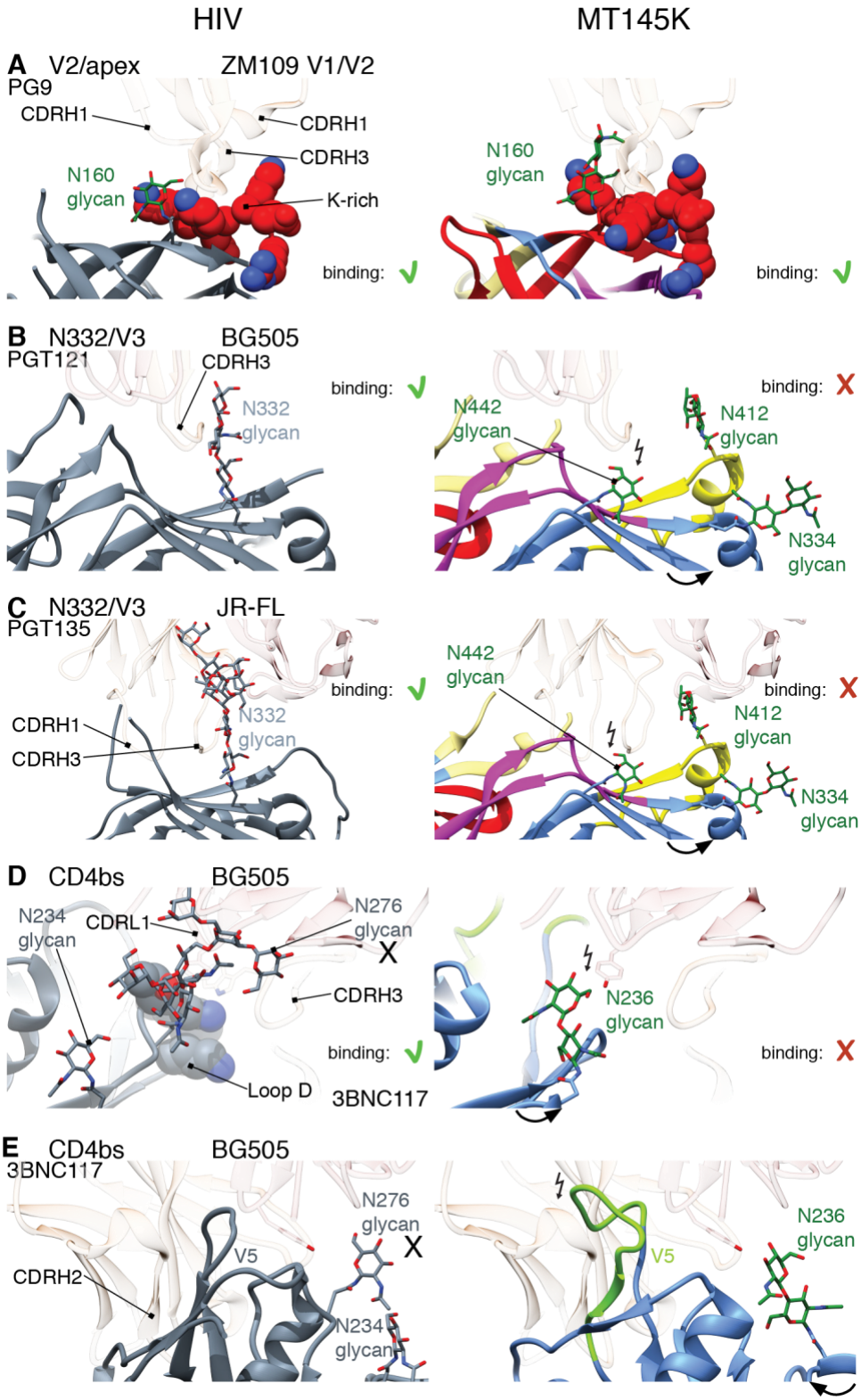

Figure S8. Molecular details of the regions on the MT145K trimer that correspond to bnAb epitopes on HIV trimers. Related to Figure 5.

A. Crystal structure of PG9 (PDB: 3U2S (McLellan et al., 2011)) bound to ZM109 V1V2-apex and docked onto BG505. The long CDRH3 of PG9 interacts with the K-rich region of the V2-apex and the glycans at N160. Both

glycan/peptide epitope elements are conserved between MT145K and HIV BG505 Env and, hence, PG9 binds strongly to both.

B-C. Crystal structures of V3-N332 bnAbs PGT121 (5T3Z (Gristick et al., 2016)) and PGT135 (PDB: 4JM2 (Kong et al., 2013)) interacting with their epitopes at the base of the V3 loop. The N332 glycan required by these bnAbs is absent on MT145K Env and the N334 glycan is projecting away from the epitopes and is not a functional substitute. In addition, the glycans N412 and N442, the latter being unique to the SIV Env, would clash with the CDRs of these bnAbs, thus preventing interaction.

D-E. Cryo-EM reconstruction of CD4bs bnAb 3BNC117, bound to BG505 trimer (PDB: 5V8M (Lee et al., 2017)). The lack of 3BNC117 binding with MT145K SIV Env trimer correlates with significant sequence variation in loop D and a clash of bnAb CDR loops with the N236 glycan that is unique to SIV. Moreover, a longer MT145 V5 loop would introduce a clash with 3BNC117 CDRH2.

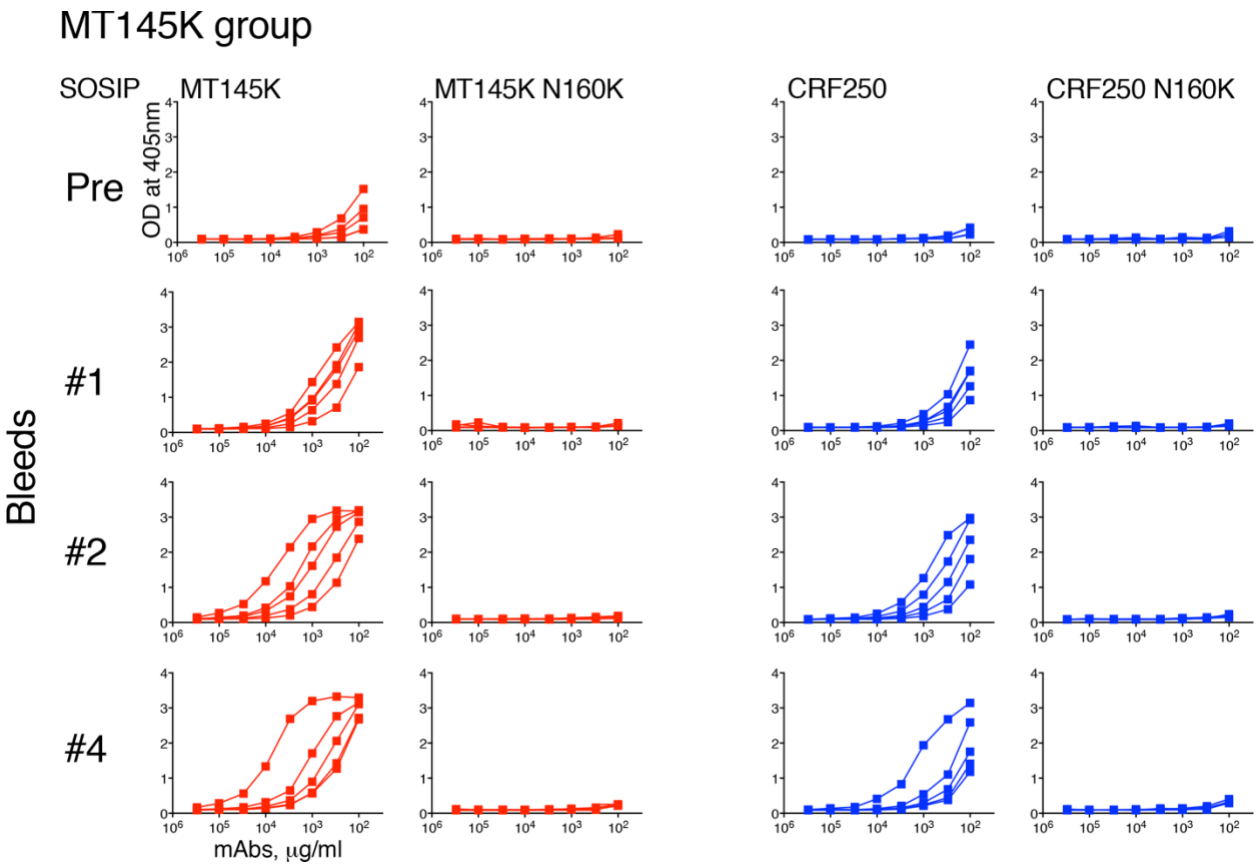

Figure S9. ELISA binding of the trimer immunized serum immune responses. Related to Figure 6.
ELISA binding curves of the MT145K trimer and HIV Env cocktail trimer-immunized CH01 UCA "HC-only" KI mice serum samples (pre-bleed (Pre), two-weeks post prime (Bleed #1), two-weeks post boost-1 (Bleed #2) and two-weeks post boost-2 (Bleed #4)) with soluble MT145K, CRF250 SOSIPs and their glycan knock-out variant (N160K) trimer proteins. Mice were immunized twice (Prime: week-0 and Boost-1: week-4) with MT145K trimer followed by boosting (boost-2 at week-8) with a 3 HIV Env-derived trimer cocktail (C108, WITO and ZM197-ZM233V1V2). Serum antibody responses mapped to the N160 glycan (part of the V2-apex bnAb core epitope) at all the immunization steps.

Map	MT145K
Data collection	
Microscope	FEI Titan Krios
Voltage (kV)	300
Detector	Gatan K2 Summit
Recording mode	Counting
Magnification (incl. post-magnification)	49,020
Movie micrograph pixelsize (Å)	1.02
Dose rate (e^-/[(camera pixel)*s])	10
Number of frames per movie micrograph	50
Frame exposure time (ms)	200
Movie micrograph exposure time (s)	10
Total dose ($e^-/Å^2$)	94
Defocus range (μm)	1.0-3.6
EM data processing	
Number of movie micrographs	1,281
Number of molecular projection images in map	44,301
Symmetry	C3
Map resolution (FSC 0.143; Å)	4.1
Map sharpening B-factor ($Å^2$)	-130
Structure Building and Validation	
Number of atoms in deposited model	15,192
gp120	3,547
gp41	964
glycans	553
MolProbity score	1.72 (88%)
Clashscore	3.55
EMRinger score	2.26
Deviations from ideal	
Bond length outliers	0 (0%)
Bond angles outliers	0 (0%)
Ramachandran plot	
Favored (%)	88.9
Allowed (%)	10.5
Outliers (%)	0.5

Table S1. Cryo-EM and model refinement statistics. Related to Figure 2.
Key statistics of cryo-EM data processing as well as model building and validation.

					MT145K group: Prime-MT145K (wk-0), Boost-1-MT145K (wk-4) and Boost-2 (wk-8) Cocktail of 3 HIV-1 trimers																											
				Ab	Pre-bleed (wk-0)						Bleed #1 (wk-2)						Bleed #2 (wk-6)						Bleed #3 (wk-8)						Bleed #4 (wk-10)					
Type	Virus/mutant	Subtype	Tier	CH01	13200	13201	13202	13300	13301		13200	13201	13202	13300	13301		13200	13201	13202	13300	13301		13200	13201	13202	13300	13301		13200	13201	13202	13300	13301	
Autologous	MT145K	SIV	2	0.173	<100	<100	<100	<100	<100		<100	<100	<100	<100	<100		109	121	<100	135	576		<100	<100	<100	<100	340		<100	109	452	220	1788	
	MT145K N160A	SIV	2	>10	<100	<100	<100	<100	<100		<100	<100	<100	<100	<100		<100	<100	<100	<100	<100		<100	<100	<100	<100	<100		<100	<100	<100	<100	<100	
Boost 2 matched	WITO	B	2	0.019	173	162	<100	145	302		205	476	241	606	1095		313	1492	529	800	2846		270	350	320	310	650		105	309	300	196	1523	
	C108	AE	2	0.028	<100	<100	<100	<100	<100		201	284	<100	<100	412		122	123	138	444	1413		<100	<100	149	190	890		113	182	254	229	2744	
	ZM233	C	2	0.035	<100	<100	<100	<100	<100		<100	<100	<100	<100	<100		122	199	595	195	536		<100	<100	<100	<100	<100		<100	110	302	<100	191	
CH01 sensitive	Q23_17	A1	1B	0.012	<100	<100	<100	<100	<100		116	383	165	369	427		197	635	260	1397	6536		153	477	471	562	3725		107	633	605	1398	>10000	
	CRF250	AG	2	0.027	<100	<100	<100	<100	<100		<100	142	150	142	255		150	285	221	165	1077		<100	<100	130	<100	289		<100	<100	318	104	738	
	CNE58	C	2	0.047	<100	<100	<100	<100	<100		<100	<100	<100	<100	<100		<100	<100	<100	<100	252		<100	<100	<100	<100	<100		<100	<100	126	<100	406	
	BG505	A	2	0.517	<100	<100	<100	<100	<100		<100	<100	<100	<100	<100		<100	<100	<100	<100	<100		<100	<100	<100	<100	<100		<100	<100	270	<100	108	
Global panel	CE703010217_B6	C	2 or 3	0.160	<100	<100	<100	<100	<100		<100	<100	<100	<100	<100		<100	113	109	<100	462		<100	<100	<100	<100	<100		<100	<100	209	115	802	
	X2278_C2_B6	B	2	0.049	<100	<100	<100	<100	<100		<100	<100	<100	<100	112		200	147	342	<100	199		<100	<100	<100	<100	<100		<100	<100	151	<100	107	
	CE1176_A3	C	2	0.072	<100	<100	<100	<100	<100		<100	<100	<100	<100	127		<100	<100	167	<100	128		<100	<100	<100	<100	<100		<100	<100	115	<100	<100	
	398_F1_F6_20	A1	1	0.316	<100	<100	<100	<100	<100		<100	<100	<100	<100	<100		<100	<100	<100	<100	<100		<100	<100	<100	<100	<100		<100	<100	154	<100	<100	
	246_F3_C10_2	A1C	2	0.981	<100	<100	<100	<100	<100		<100	<100	<100	<100	<100		<100	<100	<100	<100	<100		<100	<100	<100	<100	<100		<100	<100	109	<100	<100	
	25710_2_43	C	1B or 2	1.759	<100	<100	<100	<100	<100		<100	<100	<100	<100	<100		<100	<100	<100	<100	<100		<100	<100	<100	<100	<100		<100	<100	<100	<100	<100	
	CH119_10	07 BC	2	1.820	<100	<100	<100	<100	<100		<100	<100	<100	<100	<100		<100	<100	<100	<100	<100		<100	<100	<100	<100	<100		<100	<100	<100	<100	<100	
	X1632_S2_B10	G	2	1.973	<100	<100	<100	<100	<100		<100	<100	<100	<100	<100		<100	<100	<100	<100	<100		<100	<100	<100	<100	<100		<100	<100	<100	<100	<100	
Control	MLV4.3			>10	<100	<100	<100	<100	<100		<100	<100	<100	<100	<100		<100	<100	<100	<100	<100		<100	<100	<100	<100	<100		<100	<100	<100	<100	<100	
	MT145-WT	SIV	2	ND	<100	<100	<100	<100	<100		<100	<100	<100	<100	<100		<100	<100	<100	<100	<100		<100	<100	<100	<100	<100		<100	<100	<100	<100	<100	
	CRF250 N160A	AG	2	>10	<100	<100	<100	<100	<100		<100	<100	<100	<100	<100		<100	<100	<100	<100	<100		<100	<100	<100	<100	<100		<100	<100	<100	<100	<100	

Table S2. Serum ID50 neutralizing antibody responses of the CH01 UCA HC-only knock-in mice immunized with the chimpanzee SIV MT145K trimer followed by HIV 3-trimer cocktail boosting. Related to Figure 7.

A group of 5 CH01 UCA HC-only knock-in mice (3 heterozygous (Het) (13200, 13201 and 13202) and 2 homozygous (Hom) (13300 and 13301) for the Ig heavy chain locus (HC)) were prime-boost immunized (prime: week-0 and boost-1: week-4), with chimpanzee MT145K trimer. The animals were further boosted (boost-2 at week-8) with an HIV Env derived 3-trimer cocktail (C108, WITO and ZM197-ZM233V1V2). The mice were immunized with 25µg of the individual trimer or HIV 3-trimer cocktail (25µg total protein) with GLA-SE as adjuvant. Neutralization of the pre- and post-immune sera were carried out against a panel of viruses in the TZM-bl reporter cell assay. The numerical values in the table represent ID_{50} neutralization titers of the pre-bleed (Pre) and post-prime (Bleed #1), post boost-1 (Bleed #2), post boost-1 prior to HIV trimer boosting (Bleed #3), and post boost-2 (Bleed #4) serum samples. Neutralization was assessed against the priming immunogen-matched autologous virus, MT145K and its N160 glycan knock-out variants, boosting immunogen-matched, CH01 Ab sensitive, and global panel HIV Env-encoding viruses. The numerical values shown in the table represent the ID_{50} serum neutralization titers and were calculated by non-linear regression method from the percent neutralizations of serum titrations with virus. The ID_{50} values of <100 indicate that 50% of neutralization was not achieved for the respective serum-virus combinations at the lowest dilution (1:100) tested in neutralization assay. The IC_{50} neutralization titers for the CH01 mature Ab against the virus panel are shown.